NASA TN D-1638

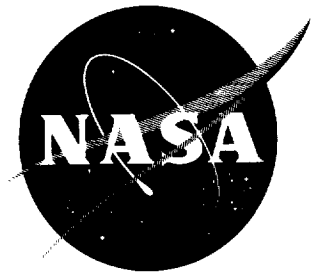

TECHNICAL NOTE

D-1638

LONGITUDINAL AERODYNAMIC CHARACTERISTICS OF SEVERAL FIFTH-STAGE SCOUT REENTRY VEHICLES FROM MACH NUMBER 0.60 TO 24.4 INCLUDING SOME REYNOLDS NUMBER EFFECTS ON STABILITY AT HYPERSONIC SPEEDS

By Patrick J. Johnston

Langley Research Center
Langley Station, Hampton, Va.

NATIONAL AERONAUTICS AND SPACE ADMINISTRATION
WASHINGTON
May 1963

Code-1

NATIONAL AERONAUTICS AND SPACE ADMINISTRATION

TECHNICAL NOTE D-1638

LONGITUDINAL AERODYNAMIC CHARACTERISTICS OF SEVERAL FIFTH-STAGE SCOUT REENTRY VEHICLES FROM MACH NUMBER 0.60 TO 24.4 INCLUDING SOME REYNOLDS NUMBER EFFECTS ON STABILITY AT HYPERSONIC SPEEDS

By Patrick J. Johnston

SUMMARY

15694

Longitudinal static stability investigations of several proposed configurations of the fifth-stage Scout reentry vehicle have been conducted in the Mach number interval from 0.60 to 24.4. The results were summarized to show the effect of varying Mach number on the normal-force-curve slope and zero-lift center of pressure. The effect on longitudinal stability of limited variations in nose shape as well as afterbody geometry were determined at a Mach number of 6.8. The low-angle-of-attack stability of one configuration was examined to determine whether the test results obtained in helium were representative of those obtained in air at Mach numbers near 20. Of the three parameters investigated (Mach number, Reynolds number, and specific heat ratio of the test medium), it appeared that Reynolds numbers had the greatest effect on longitudinal stability at low angles of attack.

INTRODUCTION

The simulation of actual flight conditions in wind tunnels is seldom achieved; indeed, in recent years, it has become practically impossible to duplicate all of the conditions a vehicle would experience, for instance, upon entering and traversing the earth's atmosphere at near orbital speed. To circumvent the formidable problems of high temperatures and pressures associated with operating and obtaining reliable data from wind tunnels at these high speeds and to duplicate conditions which, for example, a lunar vehicle would encounter upon entering the earth's atmosphere at supercircular velocities, the National Aeronautics and Space Administration is conducting a flight research program with the solid-fuel Scout rocket.

Briefly, this program has several objectives among which are the measurement of total and radiative heat transfer and a determination of the performance of thermal-protection specimens during atmospheric reentry on ballistic paths at velocities approaching 30,000 feet per second. Heat transfer and performance

data on various heat-shield materials will be recorded onboard by means of magnetic tape and subsequently telemetered to ground stations after the payload vehicle emerges from the region of telemetry blackout. The tape playback will continue until the reentry vehicle has decelerated to subsonic speeds and impacts in the ocean. Vehicle recovery will not be attempted.

In support of this flight research program, a series of wind-tunnel tests were conducted to determine the static longitudinal stability of the originally proposed payload vehicles (as well as later versions resulting from design fixes) over a wide Mach number and Reynolds number range. In particular, it was desirable to determine the stability near zero angle of attack since this incidence would provide a symmetrical heat input over the material forming the nose of the vehicles.

The tests were conducted in the Langley 8-foot transonic pressure tunnel, the Langley Unitary Plan wind tunnel, the Langley 11-inch hypersonic tunnel, and the Langley 22-inch hypersonic helium tunnel. The Mach number range over which the data were obtained extended from 0.60 to 24.4.

Some additional stability investigations were performed at hypersonic speeds on one of the 12 configurations reported on herein; these results are available in references 1 to 3. The stability data of references 1 and 3 were obtained in the Langley 24-inch hypersonic arc tunnel and the Chance Vought Corporation hypervelocity wind tunnel, respectively, at average Mach numbers of 20 and 17. Nitrogen is employed as the test medium in these hotshot-type facilities to avoid the problem of chemical reactions in the nozzles. The free-flight data of reference 2 were obtained in air at Mach numbers of approximately 5 and 17 in the Ames pressurized ballistic range and supersonic free-flight wind tunnel. The reference investigations, in addition to providing supplemental information on stability at Mach numbers near 20, afforded an opportunity to examine the air-helium simulation problem with a view toward determining whether helium facilities can usefully contribute to configuration studies at hypersonic speeds. The simulation problem has previously been examined in some detail, both theoretically (ref. 4) and experimentally (ref. 5).

SYMBOLS

C_A axial-force coefficient, $\frac{\text{Total axial force}}{qS}$

C_m pitching-moment coefficient, $\frac{\text{Pitching moment}}{qSD}$

C_N normal-force coefficient, $\frac{\text{Normal force}}{qS}$

$C_{N,\alpha}$ initial normal-force-curve slope, $\frac{dC_N}{d\alpha}$, per degree

D reference diameter, in. (see fig. 1)

M free-stream Mach number

q free-stream dynamic pressure

R_D Reynolds number based on reference diameter

S cross-sectional area based on model reference diameter

x_{cp} center-of-pressure location, inches from nose

α angle of attack, deg

Model Components:

B body

N nose

F flare

CONFIGURATIONS

The five-stage Scout program was designed to obtain basic data on atmospheric reentry phenomena at supercircular velocities. By way of introduction, the ensuing sections briefly outline the general design concepts and contain brief descriptions of the experimental payloads that have been planned - one for each flight - on which will be measured total heat transfer, radiative heat transfer, and the effectiveness of a charring ablator as a thermal protective system. The model configurations, designated herein by letter symbols and numerical subscripts, employed in the wind-tunnel investigations over the Mach number range of 0.60 to 24.4 are indicated in the appropriate places. Initially, it was thought that the stability of only two configurations would have to be determined in the ground facilities; however, as the results became available, it was soon apparent that additional development tests would be required and eventually would necessitate a total of 12 configurations. Sketches of the 12 configurations are presented in figure 1.

General Requirements

The overall geometry chosen for the fifth-stage Scout reentry vehicles was, to a great extent, dictated by the following considerations: (1) reasonably sized nose shapes on which data could be obtained (free, for example, of edge effects), (2) sufficient volume for instrumentation, (3) minimum weight compatible with structural integrity, (4) adequate size to house the final-stage rocket motor (which, for these vehicles, incorporates a 17-inch-diameter spherical case), (5) the facility for being contained in a Scout payload ascent heat shield, and

(6) the requirement of an aerodynamically stable configuration over a wide velocity spectrum.

Following these design concepts, preliminary configurations evolved which featured a common body geometry (body B_1, fig. 1(a), for example) but incorporating nose shapes appropriate to the various experiments, specifically, the total heat transfer, the radiative heat transfer, and material payloads.

Total Heat-Transfer Payload

The initial flight experiment, or total heat-transfer payload, was designed to incorporate an Inconel nose cap as a conventional heat-sink calorimeter. Instrumentation, in the form of thermocouples, will provide information on the total heat-transfer distribution over this cap. After about 15 seconds of reentry flight, this Inconel cap is designed to melt partially, jettison, and then expose a Teflon nose to the airstream. The chief purpose of the Teflon nose is to allow the vehicle to survive the reentry so that the heat-transfer data can be telemetered.

In the wind-tunnel stability investigations the Inconel nose cap was simulated by nose shape N_2 (fig. 1(b)) and the Teflon nose was simulated by nose shape N_1 (fig. 1(a)). Since some ablation was anticipated on the prototype, particularly near the edge of the Teflon nose, two wind-tunnel models were tested at $M = 24.4$ simulating the nose both before (N_{1S}, fig. 1(e)) and after ablation has taken place (N_1). Only the latter shape was investigated at the lower Mach numbers.

Radiative Heat-Transfer Payload

The second, or radiative heat-transfer payload, features a quartz window through which the radiative component of aerodynamic heating will be measured. The quartz window is mounted in a beryllium nose about 2 inches thick and 5 inches in diameter. The perimeter of the nose is made of an ablating material to insure reentry survival. For the wind-tunnel stability investigations, the radiative heat-transfer experiment was simulated by nose shape N_3. (See fig. 1(g).)

Charring Ablator Payload

An advanced heat-shield material will be tested on the third payload in an environment which simulates some of the conditions to be encountered during the reentry of the Apollo spacecraft. Thermocouples will be imbedded in the material for the purpose of determining the thermal response at various depths. The nose shape to be employed on this flight was identical to that selected for the radiative heat-transfer experiment and was, of course, simulated by nose shape N_3 (fig. 1(g)) in the wind-tunnel stability investigation.

Afterbody Geometry

With the nose shapes essentially fixed by the various experiments, the problem remained of choosing a body shape that would satisfy the requirements previously outlined. The body initially selected to be employed on all three flight payloads was simulated in the wind-tunnel investigations by body B_1 (fig. 1(a)) and features a 9° half-angle cone frustum followed by a short cylindrical section. This particular geometry satisfied the design requirements specified earlier but, as will be subsequently shown, was not effective in providing adequate stability, particularly in the hypersonic Mach number range. Two simple alterations were made in the geometry of body B_1 for the purpose of improving its stability at hypersonic speeds. These modified afterbodies were designated B_2 (fig. 1(c)) and B_3 (fig. 1(e)).

Final Modifications

Two additional models (N_4B_4, fig. 1(h) and N_5B_5, fig. 1(i)) were also investigated in the wind-tunnel program; these configurations resulted from incorporating several engineering design modifications in their counterparts N_1B_3 and N_3B_3, respectively.

In the case of configuration N_4B_4, the radius of the spherical nose segment was decreased by about an inch on the prototype as compared with configuration N_1B_3 and, in addition, the 9° cone frustum was relocated somewhat closer to the nose. The principal result of these modifications was the slight forward movement of the vehicle center of gravity relative to N_1B_3.

In the case of configuration N_5B_5, there were some small changes in exterior dimensions but the most significant modification (in regard to the aerodynamic stability) was the rearward shift in center of gravity compared with configuration N_3B_3. This shift, as will subsequently be shown, was sufficient to cause this shape to be unstable at hypersonic speeds in the low-angle-of-attack range and require the addition of a small afterbody flare to increase the stability at low incidences. The flare sizes investigated at $M = 24.4$ are shown in figure 1(i).

APPARATUS AND TESTS

Wind Tunnels

The results at Mach numbers from 0.60 to 1.20 were obtained in the Langley 8-foot transonic pressure tunnel. This variable-pressure facility incorporates a rectangular test section in which the top and bottom walls are slotted and thus permit a continuous variation in Mach number from low subsonic speeds up to 1.20.

The data at supersonic speeds were obtained in the Langley Unitary Plan wind tunnel which is a variable-pressure facility having two test sections approximately 4 feet square by 7 feet long. The low Mach number test section is capable of a continuous variation in Mach number from about 1.50 to 2.87 by means of an asymmetric sliding nozzle block. The same method is used to vary the Mach number from approximately 3.00 to 4.63 in the high Mach number test section.

At Mach numbers of 6.8 and 9.6, the data were obtained in the Langley 11-inch hypersonic tunnel which is a variable-pressure blowdown facility in which the stagnation temperature is elevated to prevent liquefaction of the air components in the two nozzles. Absolute humidity levels of the air were reduced below that for which condensation would occur in the test section.

The results at a Mach number of 24.4 were obtained in the Langley 22-inch helium blowdown tunnel utilizing a conical nozzle of 5° half angle. The flow produced by this nozzle has a longitudinal Mach number gradient of about 0.08 per inch and the models were located in the tunnel in such a way that the average free-stream cross-section Mach number at the nose was 24.4. Additional data were obtained at average free-stream Mach numbers of 20.2 and 21.2 in a contoured nozzle recently installed in this facility. This nozzle, incidently, was designed to produce theoretically uniform flow at a Mach number of 22. The change in Mach number for the tests in the contoured nozzle was the consequence of increasing the stagnation pressure from 1,000 pounds per square inch gage to 2,000 pounds per square inch gage which resulted in a thinning of the wall boundary layer and thereby increasing the effective expansion of the flow from the throat. Preliminary flow calibrations in this contoured nozzle indicate a negligibly small longitudinal Mach number gradient (0.004 per inch). Further details concerning this facility may be found in reference 6.

Tests

All models were mounted on sting-supported strain-gage balances. Angles of attack for most of the tests varied from about -4° to 12°; for some of the tests at $M = 24.4$ this range was extended to $\alpha = 20^\circ$. The angles of attack of the tests conducted in the Langley 11-inch hypersonic tunnel and in the Langley 22-inch helium tunnel were set by optical methods by using a small prism mounted in the model to reflect the light from a point source (located adjacent to the test-section window) on to a calibrated scale. This optical technique gives the true angle of attack regardless of the deflection of the balance and sting under load. (Some additional features of this system as employed in the Langley 22-inch helium tunnel are described in ref. 6.) The angles of attack for the tests in the Langley 8-foot and Unitary Plan wind tunnels were set mechanically by using previously obtained corrections to account for the deflections of the balance-sting assembly under load.

For convenient reference, the test Mach numbers and Reynolds numbers for each of the foregoing wind tunnels are listed in table I. The actual model sizes employed in the various tests can be determined from the dimensions given in figure 1 along with the appropriate scale factor presented in the table.

A comparison of the test Reynolds numbers obtained in the various ground facilities with the Reynolds number of a nominal flight trajectory is presented in figure 2. It is to be observed in this figure that exceptionally good Reynolds number simulation was achieved in several of the wind-tunnel tests, notably in the lowest Mach number range. Of perhaps greater significance was the fact that it was possible to exceed the range of flight Reynolds numbers at Mach numbers in the neighborhood of 20. It will be shown later on in this paper that the deficiency of data in the Mach number range from 10 to 15 and the relatively poor simulation of full-scale Reynolds number at Mach numbers from 5 to 10 generally precluded an exact definition of the low-incidence stability in the Mach number range from 5 to 15.

RESULTS AND DISCUSSION

Presentation of Results

The data obtained at transonic speeds on configuration N_1B_1 and N_1B_3 are presented in figures 3 and 4; results for the same configurations at supersonic Mach numbers are shown in figures 5 and 6. As indicated in table I, a number of tests were made in the Langley 11-inch tunnel to determine the effects of both nose shape as well as afterbody geometry on the stability at hypersonic speeds; these results are presented in figures 7 and 8. Data obtained at $M = 24.4$ in the Langley 22-inch helium tunnel utilizing the conical nozzle are presented in figure 9; in addition to extending the Mach number range, these tests dealt primarily with the determination of nose-corner-radius effects on stability and the effectiveness of small flares on increasing the stability of configuration N_5B_5 at hypersonic speeds. The data at $M = 20.2$ and 21.2 were obtained to determine the extent of any viscous effects on the static stability at hypersonic speeds; the results from these tests are presented in figure 10.

None of the axial-force data presented in the foregoing figures were adjusted to a condition where free-stream pressures act over the base of the model or balance cavity and, therefore, are representative of the total axial force acting on the various shapes including that due to the difference between free stream and base pressures. The omission of an axial-force adjustment also implies, of course, that the axial-force data presented herein include sting effects on the base pressures and that these effects are of undetermined magnitude.

Concerning the helium data, it may be observed that, in addition to the small effects flow angularity may have had on the low-angle-of-attack stability, the axial-force data obtained in the conical nozzle at $M = 24.4$ were somewhat lower than that measured in the contoured nozzle at approximately the same Reynolds number. (Compare figs. 9(c) and 10(b).) It is not the intent here to explain these differences but, rather, to point out that they exist and are probably associated with the flow divergence in the conical nozzle as well as the choice of employing the nose Mach number (and, consequently, a conservative value of dynamic pressure) in reducing the data to coefficient form.

During the investigation to determine the effect of Reynolds number on stability at hypersonic speeds, the sting diameter remained approximately constant while the model size was reduced from 1/4 to 1/16 scale. This reduction in model size relative to the sting meant that the support interference effects on C_A were probably greater on the 1/16-scale model than on the 1/8- and 1/4-scale models. However, since the nose contribution to the total axial force was so large, the relative change in axial force due to interference effects was, in all likelihood, a small percentage of the total force.

A summary of the basic results obtained in the investigation illustrating the effect of Mach number, Reynolds number, and several configuration variables on the static longitudinal stability is presented in figures 11 to 16. With the exception of figure 12, the data for all the tests were reduced to coefficients by employing the specific model maximum diameter and cross-sectional area as reference lengths and areas.

Exploratory Results

Nose shape N_1, which was designed to survive atmospheric reentry, was combined with the originally selected afterbody B_1 to provide a suitable configuration on which preliminary stability results could be obtained. A summary of the results obtained on models of this configuration is presented in figure 11 to indicate the effects of Mach number on the initial normal-force-curve slope and zero-lift center of pressure. Concerning the center-of-pressure data, it is pointed out that the locations were determined by measuring the slope dC_m/dC_N at zero lift and are expressed in terms of reference diameters from the nose.

The results in figure 11(a) indicate a general reduction in normal-force-curve slope throughout the Mach number interval from 0.60 to 6.8. The rapid decrease in $C_{N,\alpha}$ near sonic velocity is typical of these blunt-nosed bodies and is caused by flow separation and adverse loadings over the body.

The variation with Mach number of the zero-lift center of pressure of configuration N_1B_1 is shown in figure 11(b). The design center-of-gravity location has been indicated on the ordinate of the figure; this is a representative center-of-gravity position when the vehicle reenters the atmosphere after the fuel in the fifth-stage motor has been expended.

It is observed in figure 11(b) that the configuration is unstable throughout the Mach number range from 0.60 to 6.8. The indication of stability at the lowest Mach number is fortuitous and arises as a consequence of nonlinear force and pitching-moment characteristics at these speeds, particularly at low angles of attack. (See figs. 3(a) and 3(c).) Previous investigations (ref. 7, for example) have shown that these nonlinearities are the result of separation and, under some conditions, subsequent reattachment as the flow attempts to negotiate the abrupt expansion at the edge of the nose. Although the stability of configuration N_1B_1 was not determined at Mach numbers greater than 6.8, a reasonable extrapolation

of the results shown in figure 11(b) indicate the probability that this shape would be unstable throughout the anticipated flight Mach number range.

An apparent anomalous behavior was observed in the center-of-pressure location as the Mach number was increased from 3 to 4.63. A subsequent brief investigation indicated that this peculiarity was caused by circulatory wake flow impinging on the truncated cone which is to be employed on the prototype as a structural brace for the rocket-motor exhaust nozzle. These tests also showed that this stability reversal could be avoided by simply filling the cavity formed by this brace and the interior surface of the body shell.

Since the foregoing preliminary results indicated the probability that configuration N_1B_1 would be unstable throughout the intended speed range for the center of gravity indicated in figure 11(b), consideration was given to increasing the stability by adding ballast in the nose and thereby moving the center of gravity forward. Calculations showed, however, that the weight penalty involved in moving the center of gravity a sufficient distance forward would be exorbitant and thus would severely limit the desired maximum velocity of the flight vehicle.

Two afterbody modifications were suggested for improving the static stability of the vehicles at hypersonic speeds. The first of these alterations consisted of extending the cylindrical portion of the body rearward to the exit plane of the rocket nozzle. (This body is identified as B_2 in fig. 1(c).) The second modification consisted of replacing the cylindrical portion of the body by extending the truncated cone an equivalent length. This latter shape is identified as body B_3 and is illustrated in figure 1(e).

Tests were conducted at a Mach number of 6.8 to determine which of the previous modifications was most effective in improving the stability of the vehicle at hypersonic speeds; the results are compared in figure 12. It should be noted that, for the comparative purposes of this figure, the reference lengths and areas were chosen to be equivalent to that of the original body B_1.

It is apparent from the results presented in figure 12 that body B_3 was more effective in increasing the stability than body B_2. The superiority of body B_3 proved doubly important since an analysis of the weight involved in the two modifications showed body B_3 to be appreciably lighter than B_2 and therefore capable of greater maximum flight velocity.

As noted previously, three separate nose shapes will eventually be employed during the flight program to study aerodynamic heating and material performance. It was of interest therefore to determine whether these changes in nose geometry had significant effects on the aerodynamic stability, particularly at hypersonic Mach numbers. Such an investigation was performed at a Mach number of 6.8 and the results are summarized in figure 13, wherein it may be observed that little, if any, variation in stability occurs as a result of changing nose shape.

Longitudinal Stability of Configuration N_1B_3

Inasmuch as the foregoing experiments indicated, first of all, that changing the nose geometry had a negligible effect on stability at hypersonic speeds, and, secondly, that body shape B_3 would provide adequate stability at these velocities, attention was focused on configuration N_1B_3, the stability of which was determined from Mach numbers 0.60 to 24.4. A summary of the results from these tests is presented in figure 14. Data were not obtained at Mach numbers from 1.57 to 2.87 in the low Mach number test section of the Langley Unitary Plan wind tunnel since previous results on configuration N_1B_1 adequately defined the trends to be expected in aerodynamic stability over this Mach number interval.

The normal-force data in figure 14(a) indicate the erratic behavior in slope at transonic speeds similar to that previously found on configuration N_1B_1 at these Mach numbers. The reduction in normal-force-curve slope with Mach number at supersonic speeds appears to be diminishing at Mach numbers near 7 and it is worth noting that the value of $C_{N,\alpha}$ determined from tests in helium at $M = 24.4$ appears to be in reasonable agreement with data obtained at lower Mach numbers in air.

The zero-lift axial-force results obtained on models of configuration N_1B_3 are summarized in figure 14(b). Note that there is rather close agreement between the data obtained in helium at $M = 24.4$ and the data obtained in air at lower hypersonic Mach numbers.

The variation with Mach number of the zero-lift center of pressure of configuration N_1B_3 is summarized in figure 14(c). Marked changes in center-of-pressure location are observed to occur at transonic speeds as a result of the nonlinear force and moment variations with angle of attack (see fig. 4); in general, it may be said that, near sonic speeds, the shape is unstable over the angle-of-attack range investigated (fig. 4(c)). From its most forward position at low supersonic Mach numbers, the zero-lift center of pressure is observed to move rearward as the Mach number is increased throughout the supersonic range. Some scatter is evident in the results obtained at supersonic speeds and is probably within the accuracy of these particular measurements. According to the results in figure 14(c), the most rearward center-of-pressure position occurs at Mach numbers near 10 with some gradual forward movement as the Mach number is increased to 24.4. These results at hypersonic speeds should be viewed with some caution since, as will be demonstrated, factors other than Mach number can play an important role in determining the low-angle-of-attack static stability at hypersonic speeds.

In addition to the data previously discussed, figure 14(c) also indicates the center of pressure measured on the sharp-cornered configuration $N_{1S}B_3$. Prior to being exposed to aerodynamic heating, the Teflon nose of the prototype will have sharp edges; after the Inconel nose cap jettisons the Teflon nose will experience some ablation, particularly around the extremity, and the rounded-edge configuration N_1B_3 would result. In anticipation of this ablation on the nose of

the flight configuration a sharp-edge configuration ($N_{1S}B_3$) was tested at a Mach number of 24.4 to determine whether the slight change in geometry had any perceptible effect on the aerodynamic stability. The results of such an investigation are summarized in figure 14(c) where it may be noted that, for angles of attack near zero, the center of pressure can be expected to move somewhat nearer the nose as ablation takes place.

Effect of a Small Flare at Hypersonic Speeds

Initial tests at a Mach number of 24.4 indicated that configuration N_5B_5 was unstable at low angles of attack (fig. 9(d)) and, in addition, had a stable trim attitude at $\alpha = 12^\circ$. Consideration was given, therefore, to methods for improving the low-angle-of-attack stability so that trim would only occur at zero incidence. Ballasting in the nose was rejected for the reasons given previously in the discussion concerning configuration N_1B_1. Inasmuch as flared afterbodies can be an effective means of increasing stability, two short flares were designed to be tested on this configuration in order to assess their effectiveness at hypersonic speeds.

A summary of the results of the flare investigations is presented in figure 15 in the form of the variation of center-of-pressure location with angle of attack. Both flares were effective in the low-angle-of-attack range; however, it should be noted that the design center-of-gravity position indicated on the ordinate of the figure represents that of the basic configuration; the addition of more weight in the form of an afterbody flare would undoubtedly move the center of gravity somewhat more rearward of the position indicated in the figure. For this reason a flare slightly larger than F_1 might be required to provide stability in the low-angle-of-attack range.

Air-Helium Simulation

During the investigation of the stability of configuration N_1B_3, there arose some question as to whether the results obtained in helium were actually representative of conditions that would occur in flight at these Mach numbers, or, in other words, whether air simulation was achieved by the tests in helium. Concurrently, design refinements were made on configuration N_1B_3 and a somewhat modified version designated N_4B_4 resulted. These modifications, it will be recalled, consisted of a small reduction in the spherical nose radius while simultaneously moving the truncated conical body slightly forward. In view of these modifications and in recognition of the valid question concerning the simulation of air data by testing in helium, it was decided that configuration N_4B_4 (fig. 1(h)) would be employed to determine whether, in fact, reasonable air simulation was accomplished by the tests in helium.

As indicated in table I, the longitudinal stability of N_4B_4 was determined in several different facilities at Mach numbers of approximately 17, 20, and 24.

The data from the hotshot tunnels (refs. 1 and 3) were obtained in a nitrogen atmosphere (to avoid chemical reactions in the nozzle) and the free-flight data (ref. 2) were obtained in air. Both of these test media, of course, have specific heat ratios of 7/5 at standard conditions in contrast to 5/3 for helium. In addition to these results at Mach numbers near 20, one free-flight test was conducted in a ballistic range in air at $M = 5$. (See ref. 2.) A summary of these experimental data is presented in figure 16.

The normal-force-curve-slope results obtained on configuration N_4B_4 are presented as a function of Mach number in figure 16(a) wherein it may be noted that, although some scatter exists in the data, the helium results at a Mach number of 24.4 appear to give a reasonable simulation of normal-force-curve slope at hypersonic speeds. A faired curve representing previous results obtained on configuration N_1B_3 is also shown in the figure for reference purposes and to indicate the trends to be expected over the Mach number range.

The zero-lift center-of-pressure results of N_4B_4 as obtained from the various facilities are summarized in figure 16(b). Again, a fairing representing the center-of-pressure data previously obtained on configuration N_1B_3 is shown for comparison purposes. As a result of the pronounced scatter exhibited in the center-of-pressure data shown in this figure, it could not readily be determined whether the stability of configuration N_4B_4 was simulated by the test in helium. Moreover, there is no apparent Mach number correlation of the data obtained in air and nitrogen, both of which have equivalent specific heat ratios at standard conditions.

The unexpected scatter noted in figure 16(b) prompts the question of whether Mach number or even specific heat ratio is the most important parameter governing the low-angle-of-attack stability of these configurations at hypersonic speeds. Inspection of table I shows that the data presented in figure 16(b) were obtained over a considerable range in Reynolds number; consequently, it appeared worthwhile to determine whether this parameter was significantly affecting the location of the zero-lift center of pressure at hypersonic speeds.

To aid in the assessment of Reynolds number effects on low-angle-of-attack stability, additional models having scale factors of 1/16 and 1/4 were fabricated and tested over a range of Reynolds numbers from 0.48×10^6 to 3.50×10^6 in the Langley 22-inch helium tunnel; these new data are presented in figure 16(c) as a function of Reynolds number along with the results previously discussed. It is evident in the data of figure 16(c) that Reynolds number can significantly affect the low-angle stability of these blunt-nosed bodies at hypersonic speeds. Concerning the simulation problem, it is interesting to note that an extrapolation of the fairing through the helium data is in close agreement with the low Reynolds number data of reference 1 obtained in a hypersonic arc tunnel employing nitrogen as the test medium.

The center-of-pressure location as determined from tests in the Chance-Vought hypervelocity wind tunnel and reported in reference 3 is in apparent disagreement

with the trend shown in figure 16(c); the mean probable error of these pitching-moment data was relatively large, however, and this inaccuracy was likely responsible for the discrepancies in center-of-pressure location indicated in the figure. Small differences between the data obtained in helium and the hypersonic free-flight tunnel results of reference 2 at equivalent Reynolds numbers may be due to the difference in specific heat ratios of the test media (5/3 and 7/5, respectively) or to the existence of real-gas effects in the free-flight data. The techniques of data reduction as well as the accuracy of obtaining data on very small models in the supersonic free-flight tests are additional possible explanations for the small differences observed.

In view of the dependence of the hypersonic stability on Reynolds number shown in figure 16(c), the wind-tunnel data obtained in the Mach number range from about 5 to 10 must be viewed with suspicion insofar as their applicability to the prototype is concerned because of the poor simulation of full-scale Reynolds number. (See fig. 2.) For example, although the center of pressure was found to be 0.825D from the nose at $M = 9.6$, because the test Reynolds number was an order of magnitude below the nominal flight Reynolds number, it may be anticipated that, on the basis of the results in figure 16(c) the flight center of pressure might be situated somewhat forward of this location. The poor simulation of flight Reynolds numbers in the Mach number range from 5 to 10 and the lack of data in the Mach number range from 10 to 15 did not permit a precise definition of the prototype stability over this speed range. It can readily be seen, however, on the basis of the results in figure 16(c) that the prototype will be stable during the initial penetration of the atmosphere and that the static stability will diminish as deceleration takes place and the Reynolds number continues to increase to a maximum value of approximately 3×10^6 in the neighborhood of $M = 10$.

An examination of the center-of-pressure data at an angle of attack of 8° indicated that, within the experimental scatter, there was little effect of Reynolds number except, perhaps, at the very lowest value available ($R_D = 52{,}000$).

Figure 16(d) presents the initial normal-force-curve slope as a function of Reynolds number. It may be noted that, although the helium-tunnel results indicate an invariance of $C_{N,\alpha}$ with Reynolds number, the normal-force-curve slope determined in the hotshot facilities indicates a slight reduction in $C_{N,\alpha}$ with diminishing Reynolds number.

It is of interest to speculate as to the type of flow phenomena responsible for the shifts in zero-lift center of pressure with Reynolds number at hypersonic speeds. One plausible argument is that the Reynolds number variation substantially affects the local induced pressures over the body. An experimental investigation of the induced pressures on flow-alined cylindrical bodies (ref. 8) has established that these pressures are strongly dependent on Reynolds number.

Recently, a more detailed investigation of the induced-pressure problem (the preliminary results of which are shown in ref. 5) indicates that, for blunter noses, the effect of varying Reynolds number on the induced pressures is limited principally to regions near the nose-cylinder afterbody junction. Viscous effects

on induced pressures downstream of more slender noses, on the other hand, extended much farther downstream. Some, as yet unpublished, results obtained in the Langley 22-inch helium tunnel indicate similar trends on small-angle conical bodies having blunt noses. The implication of these induced-pressure measurements is that the predominant effects of viscosity are limited (because of the blunt noses) to regions not too far downstream of the nose for the shapes under consideration in the present tests. Since the results of both references 5 and 8 were limited to zero angle of attack, it is worth inquiring as to how these viscous induced pressures affect stability at hypersonic speeds.

At zero incidence, according to reference 5, the local pressures downstream of a blunt nose consist of inviscid pressures brought about by the introduction of a large amount of energy to the flow by the blunt nose (blast wave effect) and an additional increment in pressure which is dependent on Reynolds number. For the case of small angles of attack, the symmetrical loading at zero incidence is distorted; the inviscid pressures on the windward surfaces are compressed while those on the leeward surfaces are reduced by virtue of the greater expansion of the flow from the stagnation point. The incremental pressures due to viscosity, on the other hand, are not only affected by changes in angle of attack but by Reynolds number variations as well. Consider first the effects due to angle of attack: the local Reynolds numbers are increased on the windward surfaces and the viscous effects on the loading over these portions of the body are thereby suppressed; on the leeward surfaces the local Reynolds numbers are reduced and the incremental pressures due to viscous effects can become very large - indeed great enough to dominate the destablizing input of the opposing (or windward) surface pressures. As the stream Reynolds number is reduced, the contribution of these leeward surface pressures is sufficient to bring about the stabilizing input to the pitching moment and the corresponding rearward shift in center of pressure noted in figure 16(c). At higher angles of attack it is likely that the inviscid pressures due to angle of attack become large enough on the windward surfaces to prevail over the contribution of any leeward pressures due to viscous effects except, perhaps, at extremely low stream Reynolds numbers.

The principal conclusion to be drawn from these arguments is that Reynolds number may assume a more significant role than Mach number in determining the low-angle-of-attack stability of certain configurations at hypersonic speeds. The extent to which the foregoing Reynolds number dependence is affected by such variables as Mach number, nose bluntness, body geometry, fineness ratio, and angle of attack remains to be determined.

In concluding these remarks on induced-pressure effects on stability, it should be noted that all the data in the present investigation were obtained under essentially perfect gas conditions whereas the flight vehicle will experience conditions in the real-gas thermodynamic regime. The extent to which these real-gas effects might alter the present results is not yet wholly understood.

CONCLUDING REMARKS

An investigation of the stability of several proposed configurations of the fifth-stage Scout reentry vehicle has been conducted over the Mach number interval from 0.60 to 24.4. The results were summarized to show the normal-force-curve slope and zero-lift center-of-pressure variation over the Mach number range. The effect on longitudinal stability of limited variations in nose shape as well as afterbody geometry was assessed at hypersonic speeds.

The stability data of one configuration were examined in some detail to determine whether the test results in helium were representative of those obtained in air at Mach numbers in the neighborhood of 20. Of the three variables investigated (Mach number, Reynolds number, and specific heat ratio) it appeared that Reynolds number had the most important effect on the longitudinal stability near zero angles of attack.

Langley Research Center,
National Aeronautics and Space Administration,
Langley Station, Hampton, Va., January 29, 1963.

REFERENCES

1. Harrison, Edwin F.: Static Stability Tests in the Langley 24-Inch Hypersonic Arc Tunnel on a Blunted Cone at a Mach Number of 20. NASA TN D-1508, 1962.

2. Kirk, Donn B., and Miller, Robert J.: Free-Flight Tests of Fifth-Stage Scout Entry Vehicle at Mach Numbers of 5 and 17. NASA TN D-1425, 1962.

3. Pope, T. C.: Chance Vought Hypervelocity Wind Tunnel Force Tests of a Five Stage Scout Payload Re-Entry Configuration. Rep. No. HVWT-TEST 13 (Contract No. NAS 1-1438), Vought Astronautics, Chance Vought Corp., Jan 24, 1961.

4. Love, Eugene S., Henderson, Arthur, Jr., and Bertram, Mitchel H.: Some Aspects of Air-Helium Simulation and Hypersonic Approximations. NASA TN D-49, 1959.

5. Henderson, Arthur, Jr.: Recent Investigations of the Aerodynamic Characteristics of General and Specific Lifting and Nonlifting Configurations at Mach 24 in Helium, Including Air-Helium Simulation Studies. Presented at the Specialists' Meeting on the High Temperature Aspects of Hypersonic Flow (Rhode-Saint-Genese, Belgium), AGARD, Apr. 1962.

6. Johnston, Patrick J., and Snyder, Curtis D.: Static Longitudinal Stability and Performance of Several Ballistic Spacecraft Configurations in Helium at a Mach Number of 24.5. NASA TN D-1379, 1962.

7. Reese, David E., Jr., and Wehrend, William R., Jr.: An Investigation of the Static and Dynamic Aerodynamic Characteristics of a Series of Blunt-Nosed Cylinder-Flare Models at Mach Numbers From 0.65 to 2.20. NASA TM X-110, 1960.

8. Mueller, James N., Close, William H., and Henderson, Arthur, Jr.: An Investigation of Induced-Pressure Phenomena on Axially Symmetric, Flow-Alined, Cylindrical Models Equipped With Different Nose Shapes at Free-Stream Mach Numbers From 15.6 to 21 in Helium. NASA TN D-373, 1960.

TABLE I

FACILITIES USED AND MODEL CONFIGURATIONS TESTED

Wind tunnel	Test medium	Source of data	Model scale	M	R_D	N_1B_1	N_2B_1	N_1B_2	N_1B_3	$N_{1S}B_3$	N_2B_2	N_2B_3	N_3B_3	N_4B_4	N_5B_5	$N_5B_5F_1$	$N_5B_5F_2$
Langley 8-foot transonic pressure tunnel	Air	Present investigation	1/2	0.60	2.51×10^6	X			X								
			1/2	.80	2.91	X			X								
			1/2	.90	2.74	X			X								
			1/2	1.00	1.67	X			X								
			1/2	1.10	1.70	X			X								
			1/2	1.20	1.73	X			X								
Langley Unitary Plan wind tunnel	Air	Present investigation	1/2	1.57	4.73×10^6	X											
			1/2	2.00	4.24	X											
			1/2	2.40	4.58	X											
			1/2	2.87	3.91	X											
			1/2	3.00	4.22	X			X								
			1/2	3.50	3.52	X			X								
			1/2	4.00	3.73	X			X								
			1/2	4.63	4.00	X			X								
Langley 11-inch hypersonic tunnel	Air	Present investigation	1/8	6.8	0.45×10^6	X	X	X	X		X	X	X				
			1/8	9.6	.32				X			X	X				
Contour nozzle of Langley 22-inch helium tunnel	Helium	Present investigation	1/16	20.2	0.48×10^6									X			
			1/8	20.2	.96									X			
			1/4	20.2	1.93									X			
			1/4	21.2	3.50									X			
Conical nozzle of Langley 22-inch helium tunnel	Helium	Present investigation	1/8	24.4	0.71×10^6				X	X				X	X	X	X
Ames ballistic range	Air	Reference 2	1/45	5.14	0.22×10^6									X			
Chance-Vought hotshot tunnel	Nitrogen	Reference 3	0.08, 1/10	17.3	0.17×10^6									X			
Ames supersonic free-flight tunnel	Air	Reference 2	1/45	17	2×10^6 to 4×10^6									X			
Langley 24-inch hypersonic arc tunnel	Nitrogen	Reference 1	1/7	20	0.052×10^6									X			

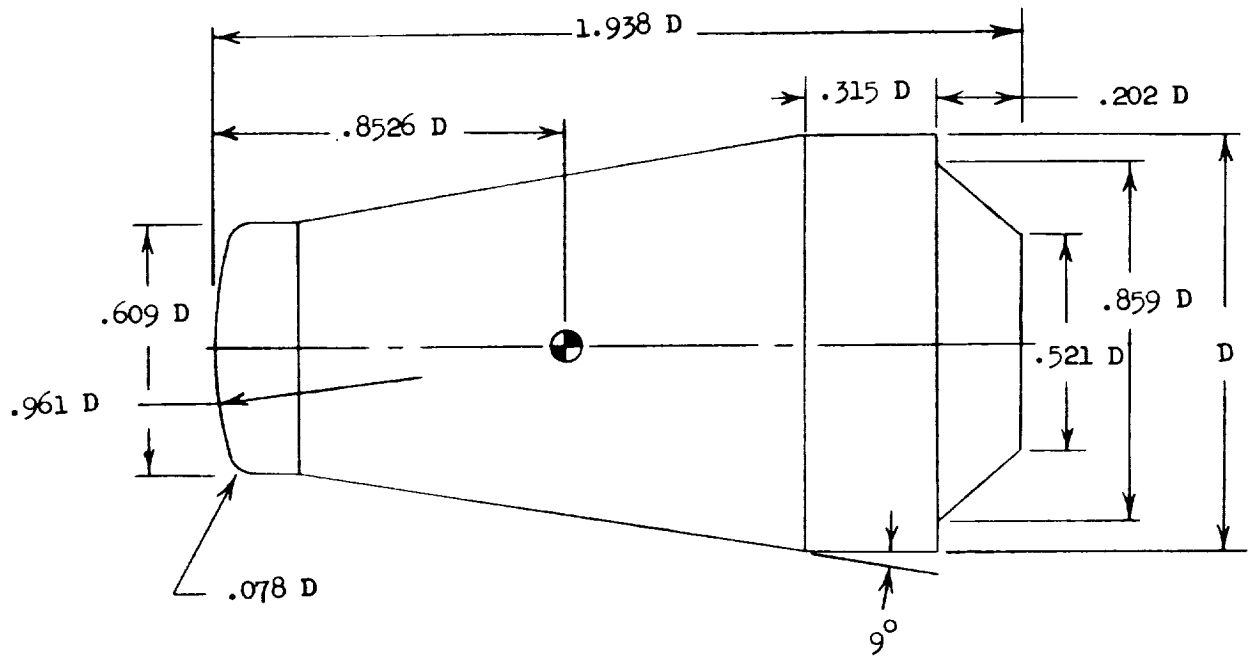

(a) N_1B_1; D = 18.25 inches full scale.

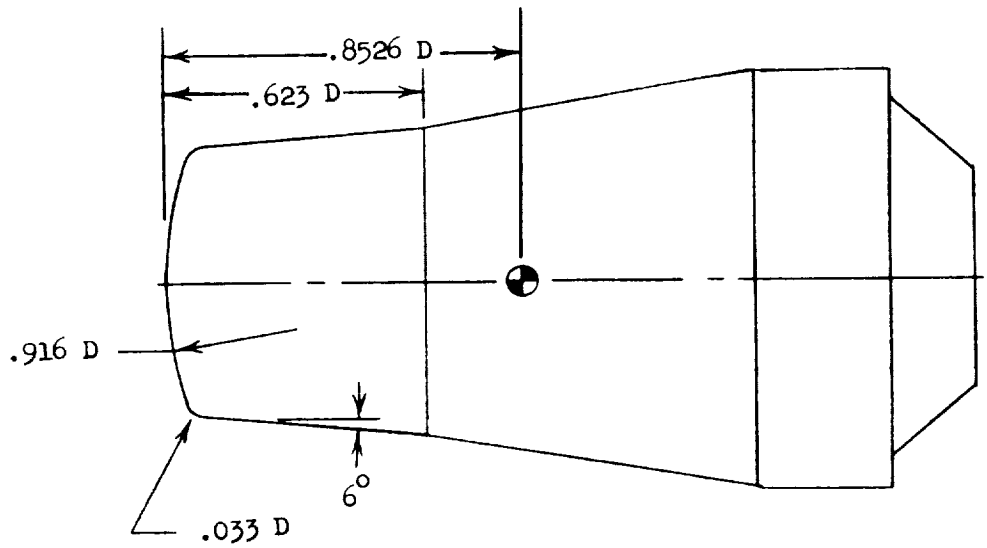

(b) N_2B_1; D = 18.25 inches full scale.

Figure 1.- Configuration dimensions in terms of reference length.

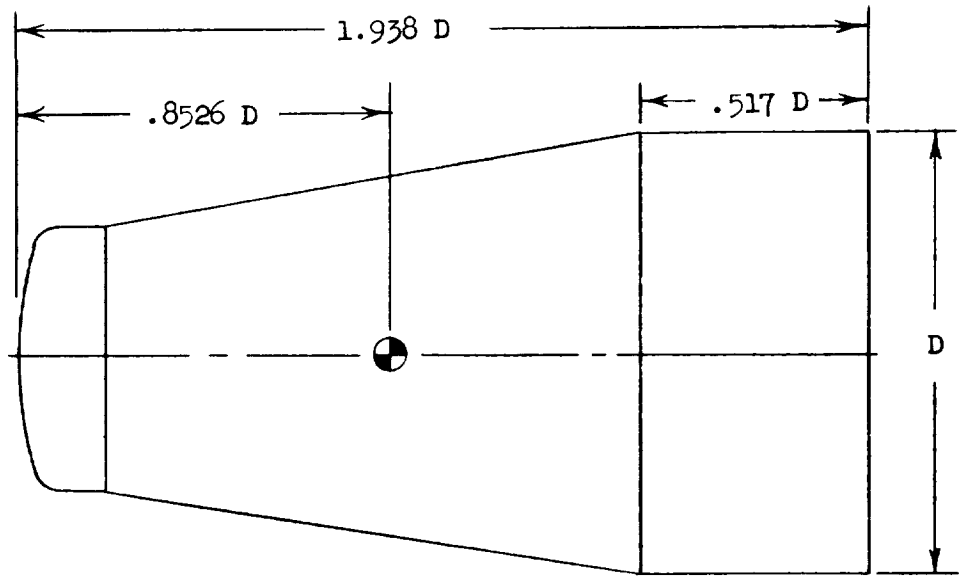

(c) N_1B_2; D = 18.25 inches full scale.

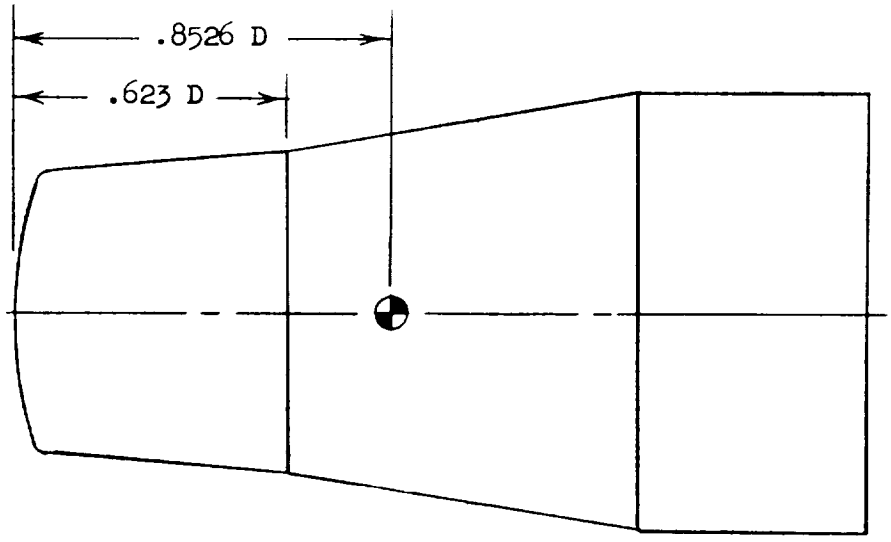

(d) N_2B_2; D = 18.25 inches full scale.

Figure 1.- Continued.

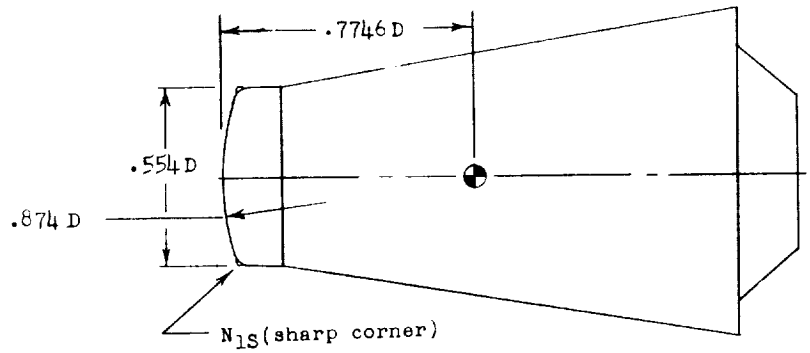

(e) N_1B_3 and $N_{1S}B_3$; D = 20.07 inches full scale.

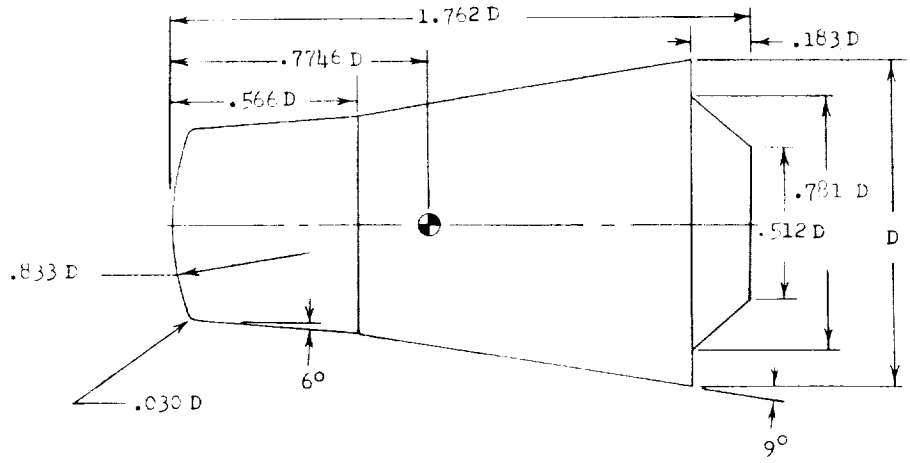

(f) N_2B_3; D = 20.07 inches full scale.

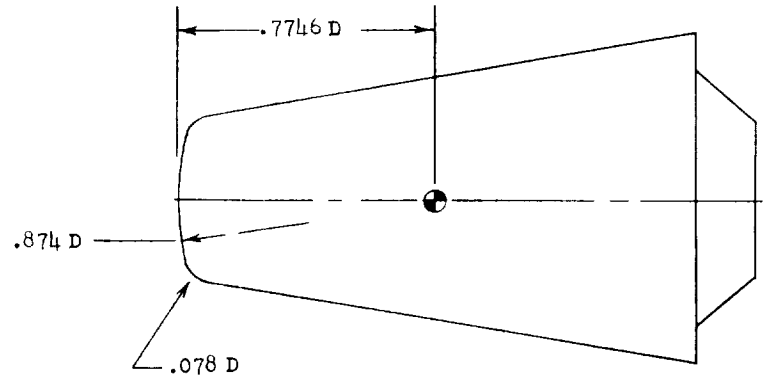

(g) N_3B_3; D = 20.07 inches full scale.

Figure 1.- Continued.

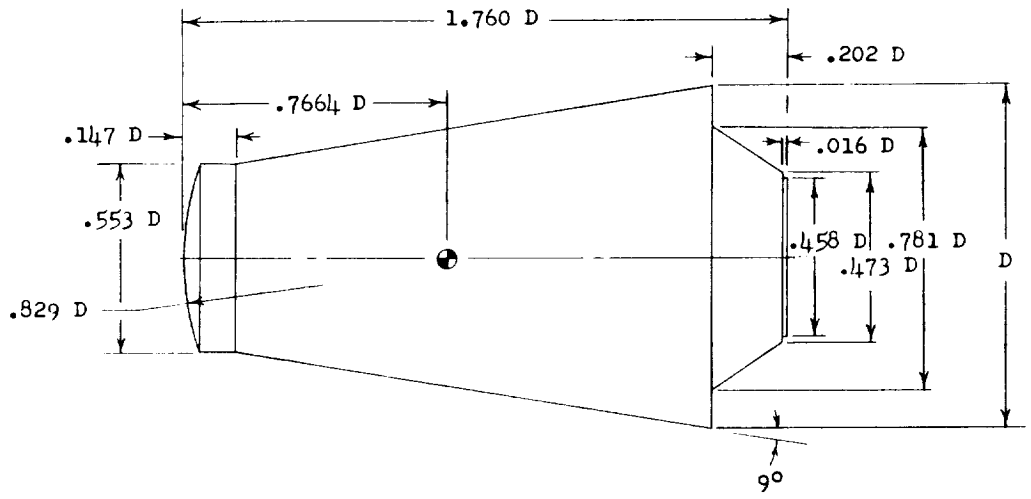

(h) N_4B_4; D = 20.07 inches full scale.

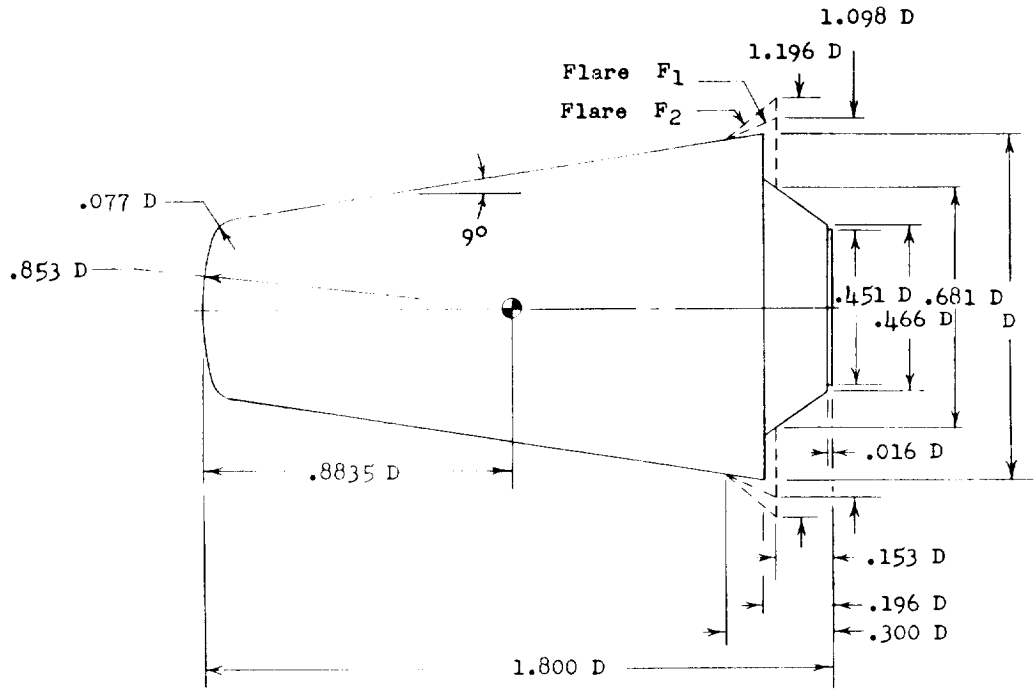

(i) N_5B_5, $N_5B_5F_1$, and $N_5B_5F_2$; D = 20.39 inches full scale.

Figure 1.- Concluded.

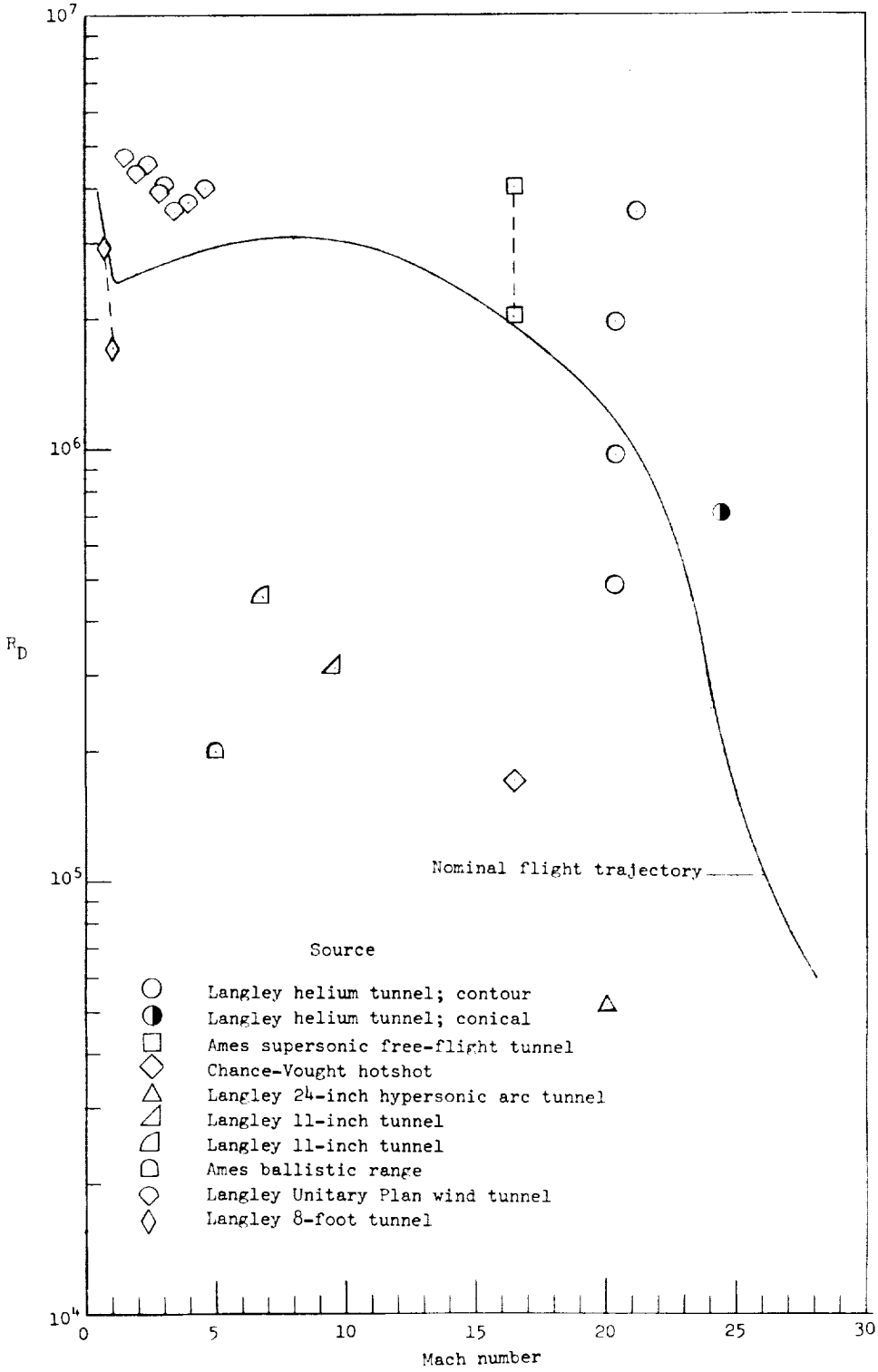

Figure 2.- A comparison of flight and wind-tunnel Reynolds numbers.

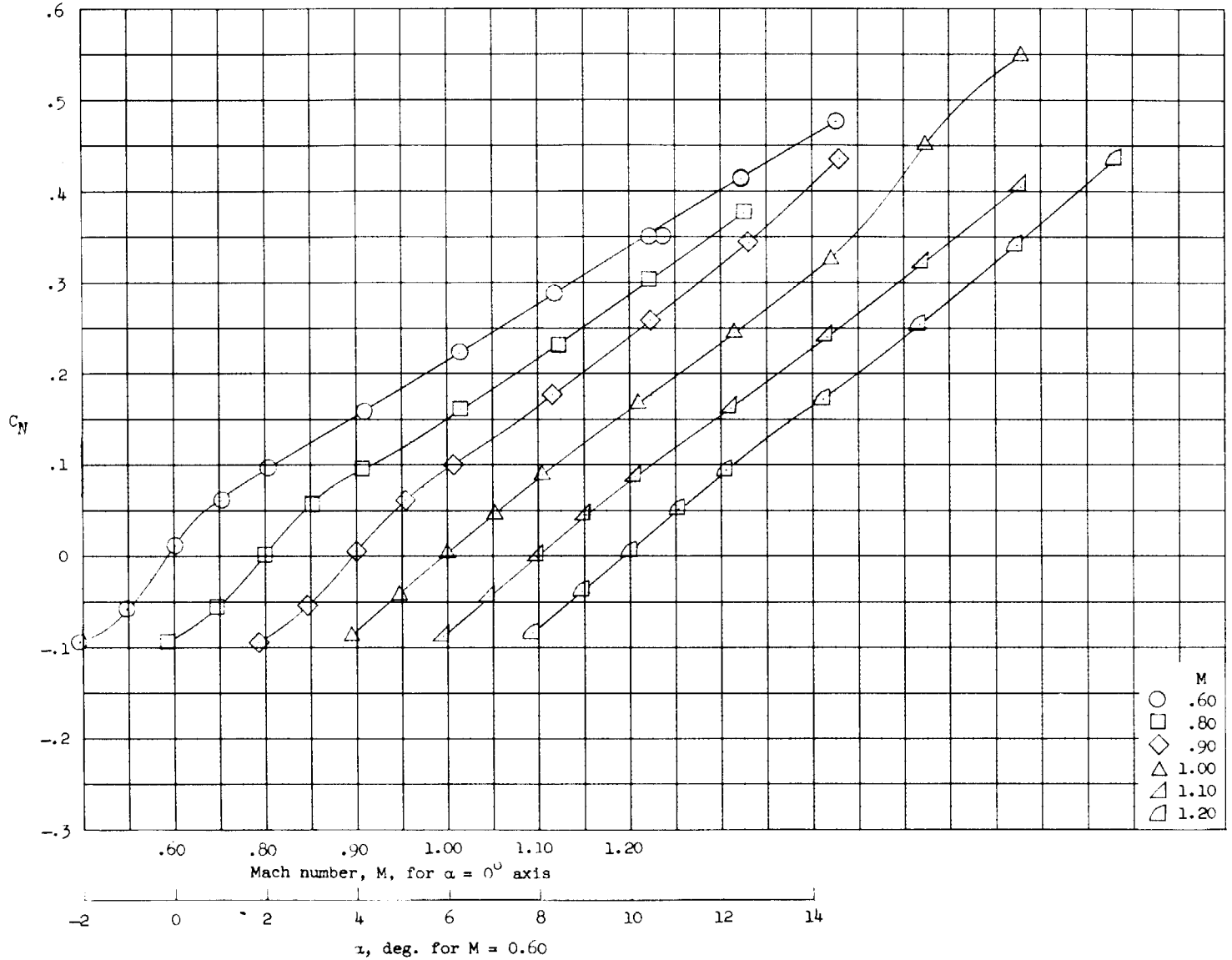

(a) C_N.

Figure 3.- Stability results at transonic speeds on configuration N_1B_1.

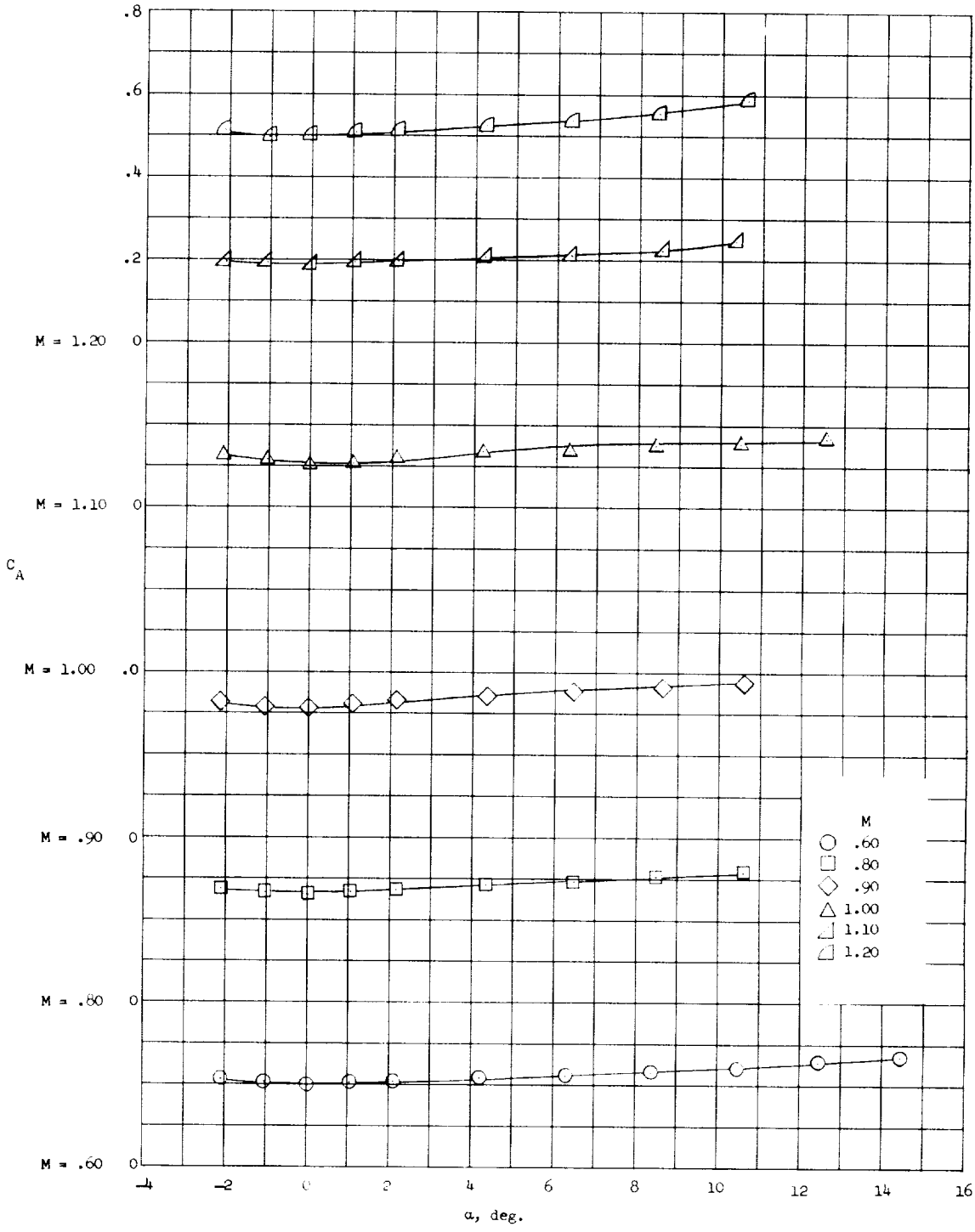

(b) C_A.

Figure 3.- Continued.

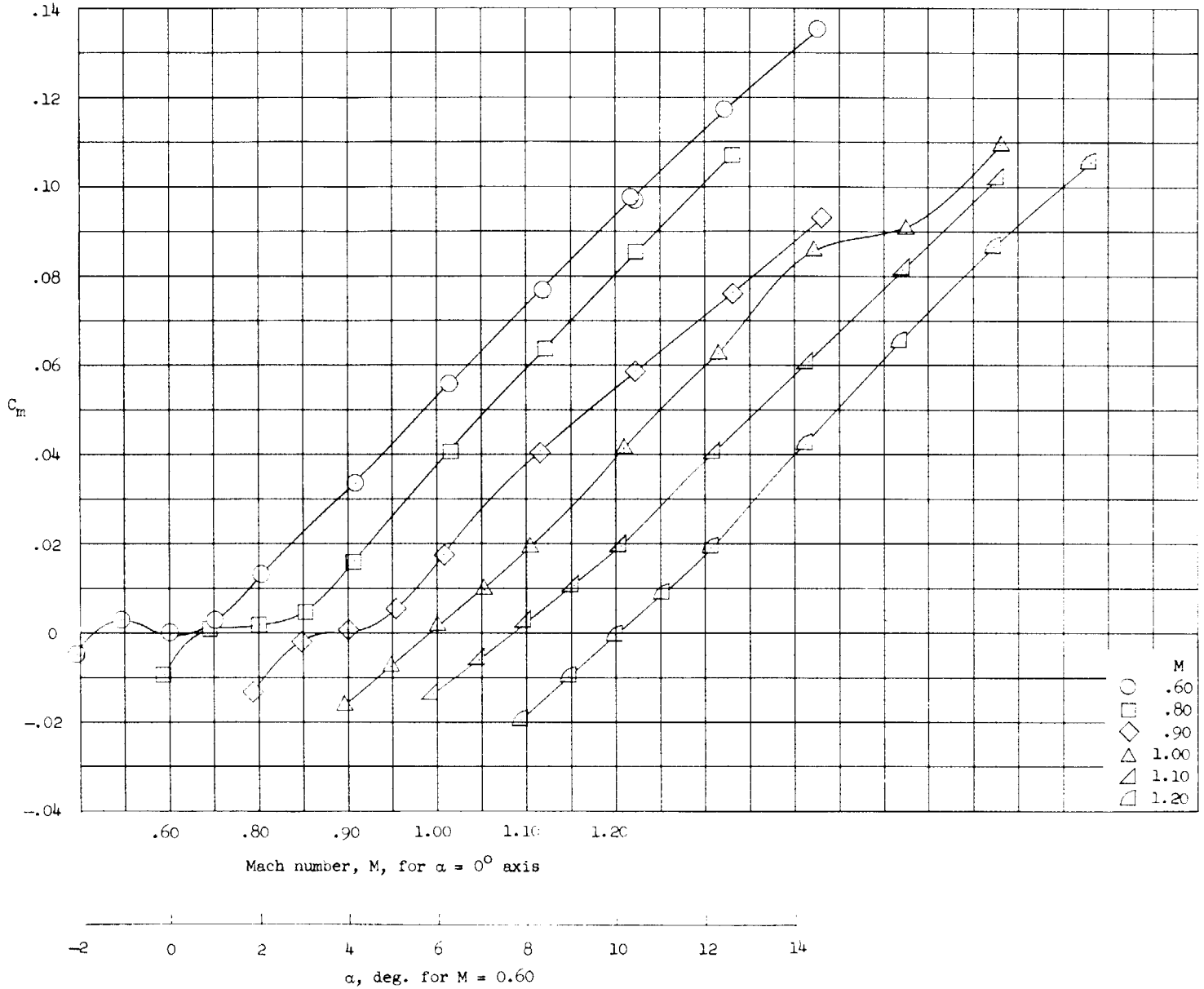

(c) C_m.

Figure 3.- Concluded.

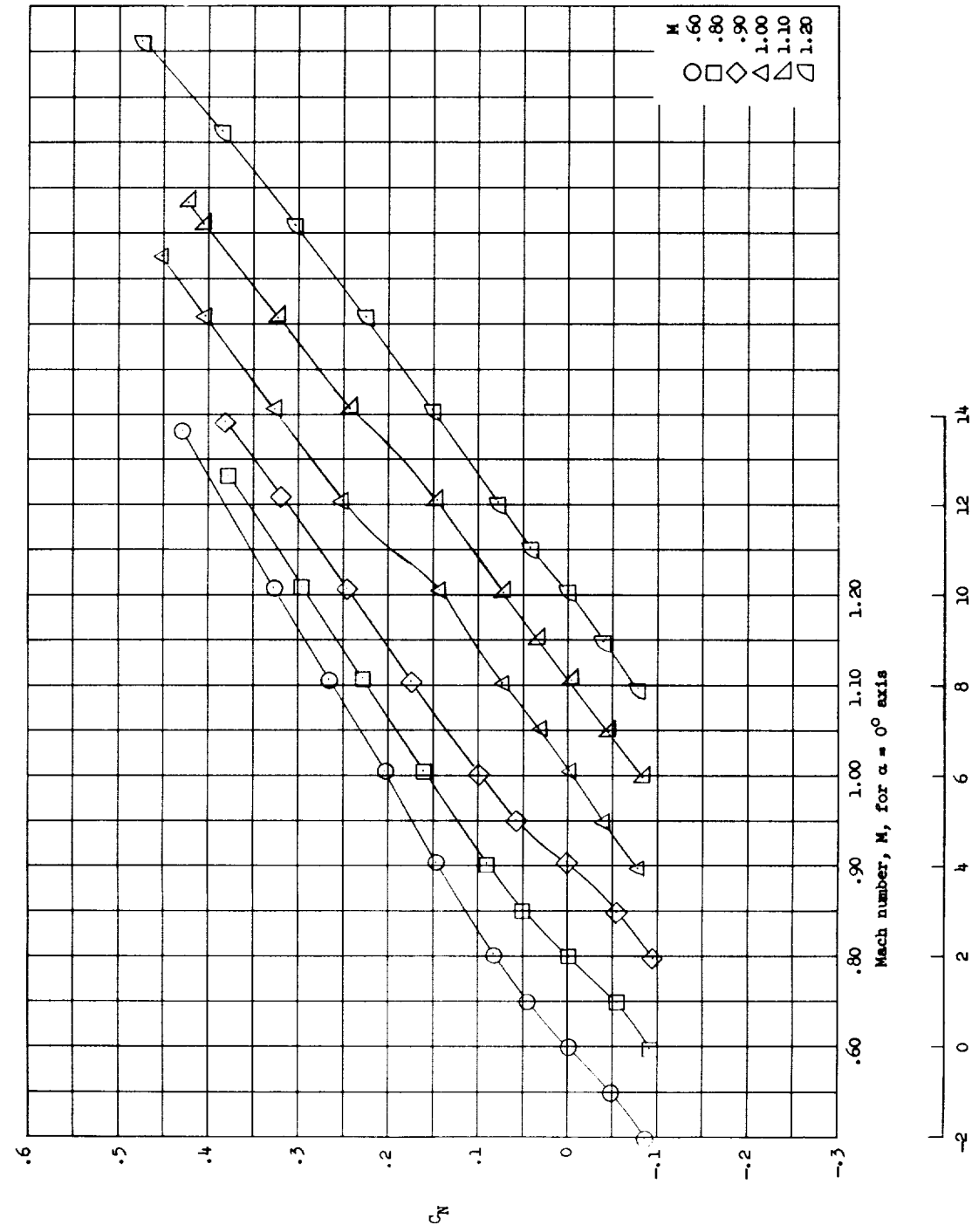

(a) C_N.

Figure 4.- Stability results at transonic speeds on configuration N_1B_3.

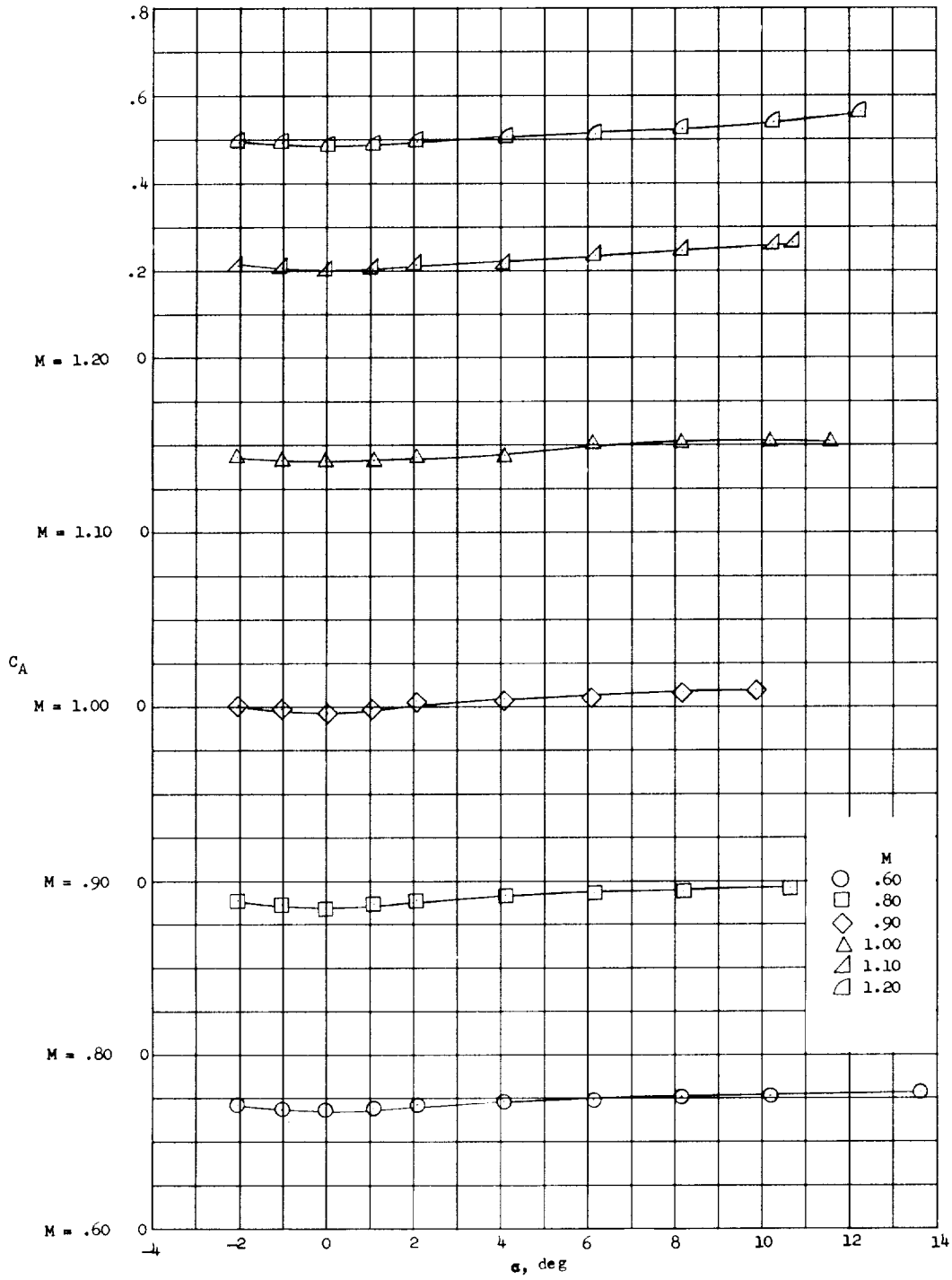

(b) C_A.

Figure 4.- Continued.

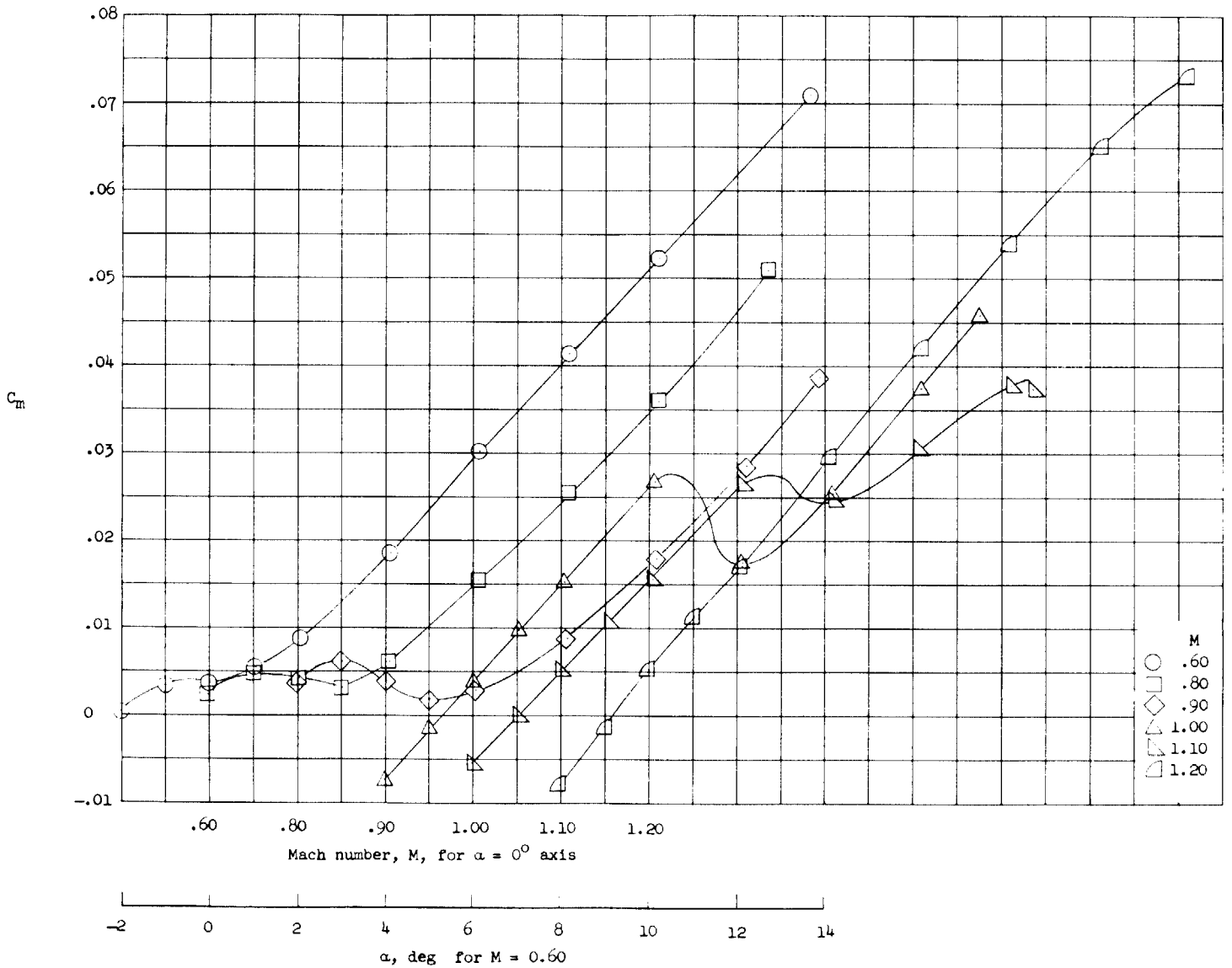

(c) C_m.

Figure 4.- Concluded.

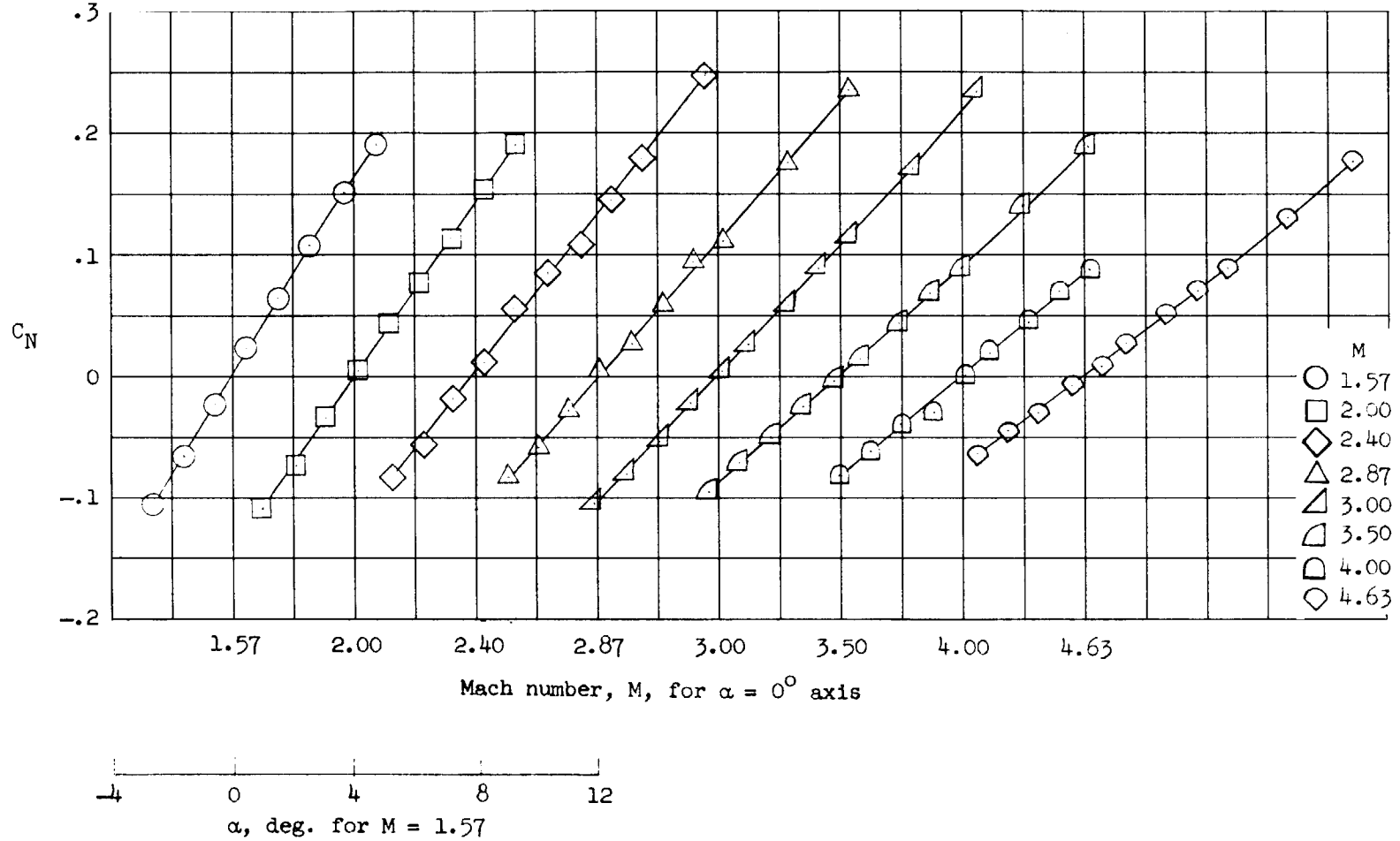

(a) C_N.

Figure 5.- Stability results at supersonic speeds on configuration N_1B_1.

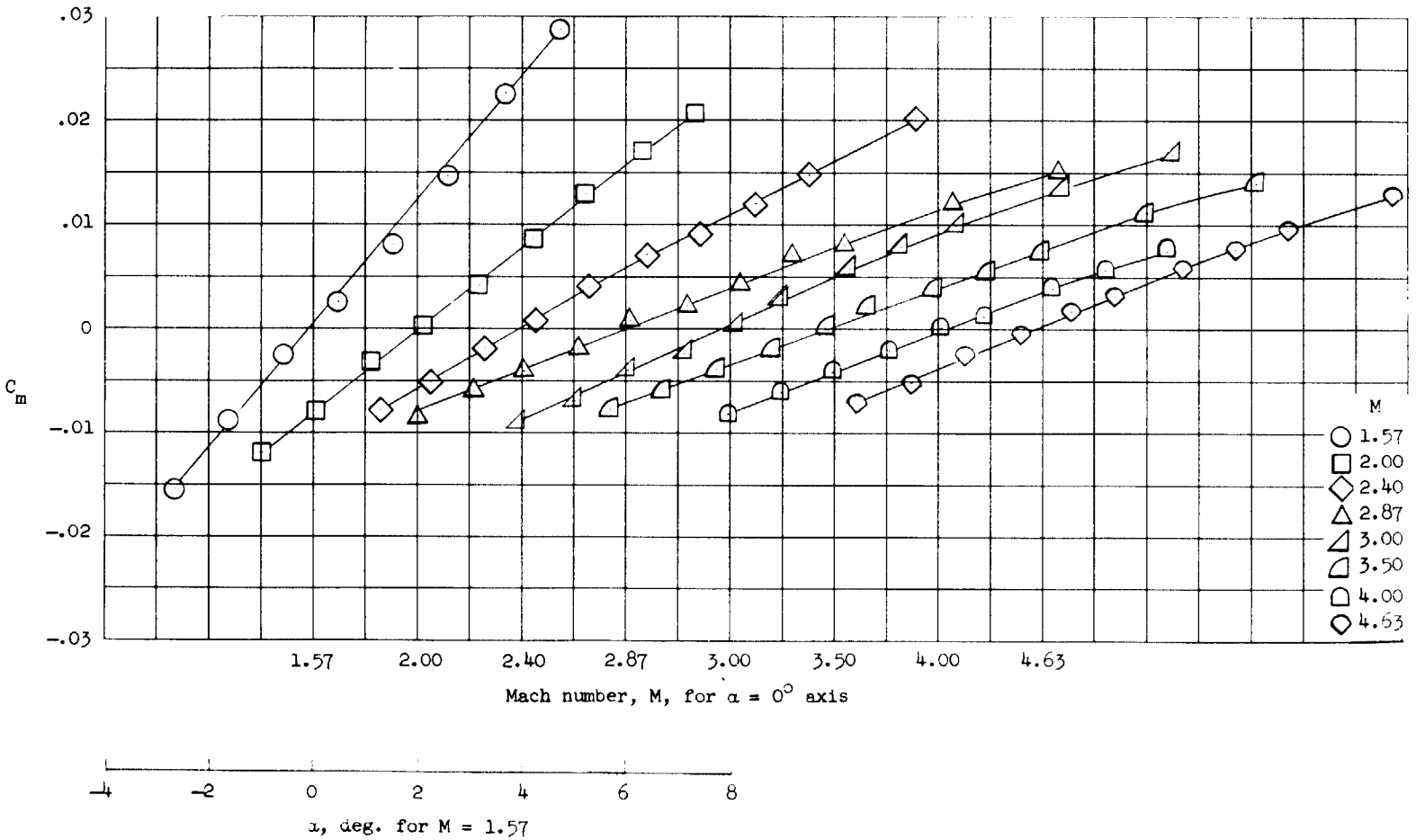

(b) C_m.

Figure 5.- Concluded.

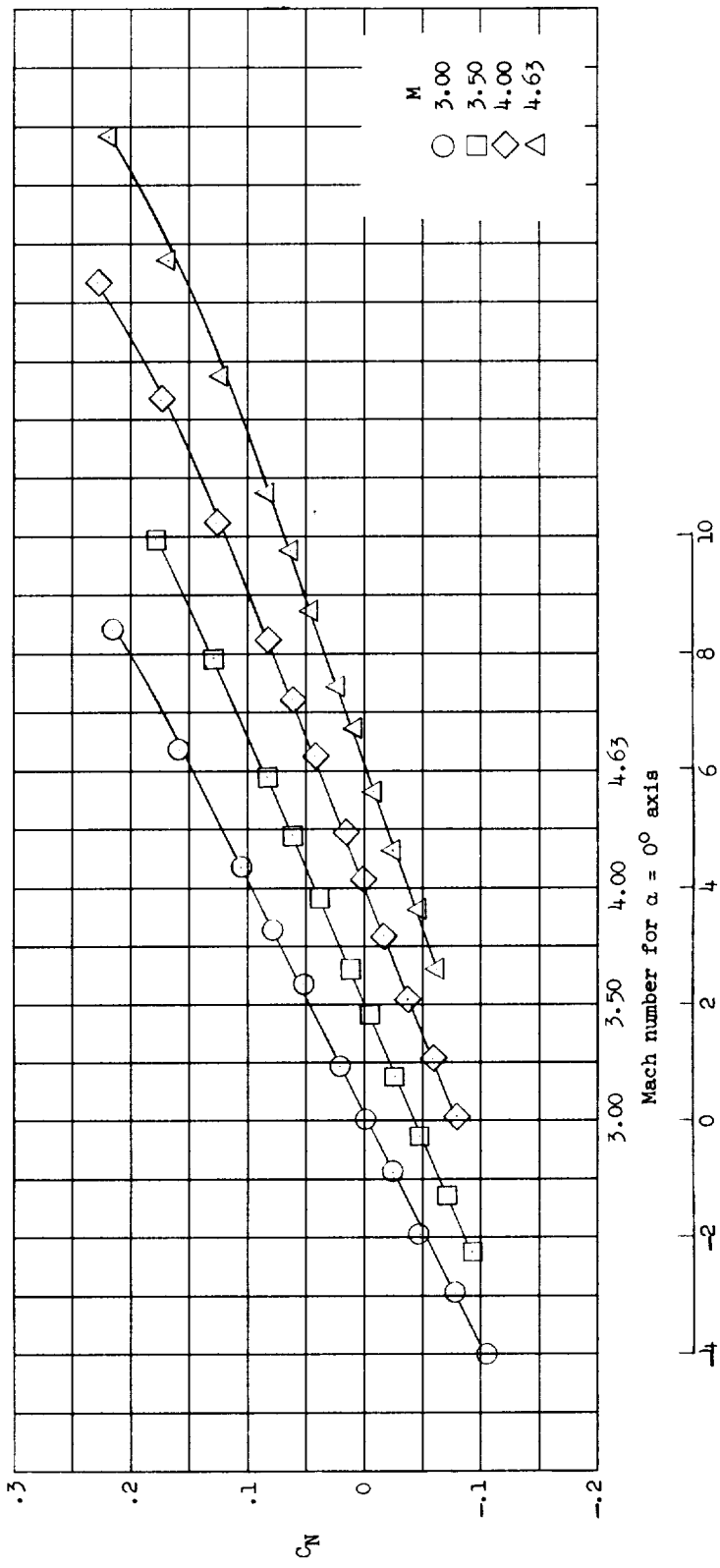

(a) C_N.

Figure 6.- Stability results at supersonic speeds on configuration N_1B_3.

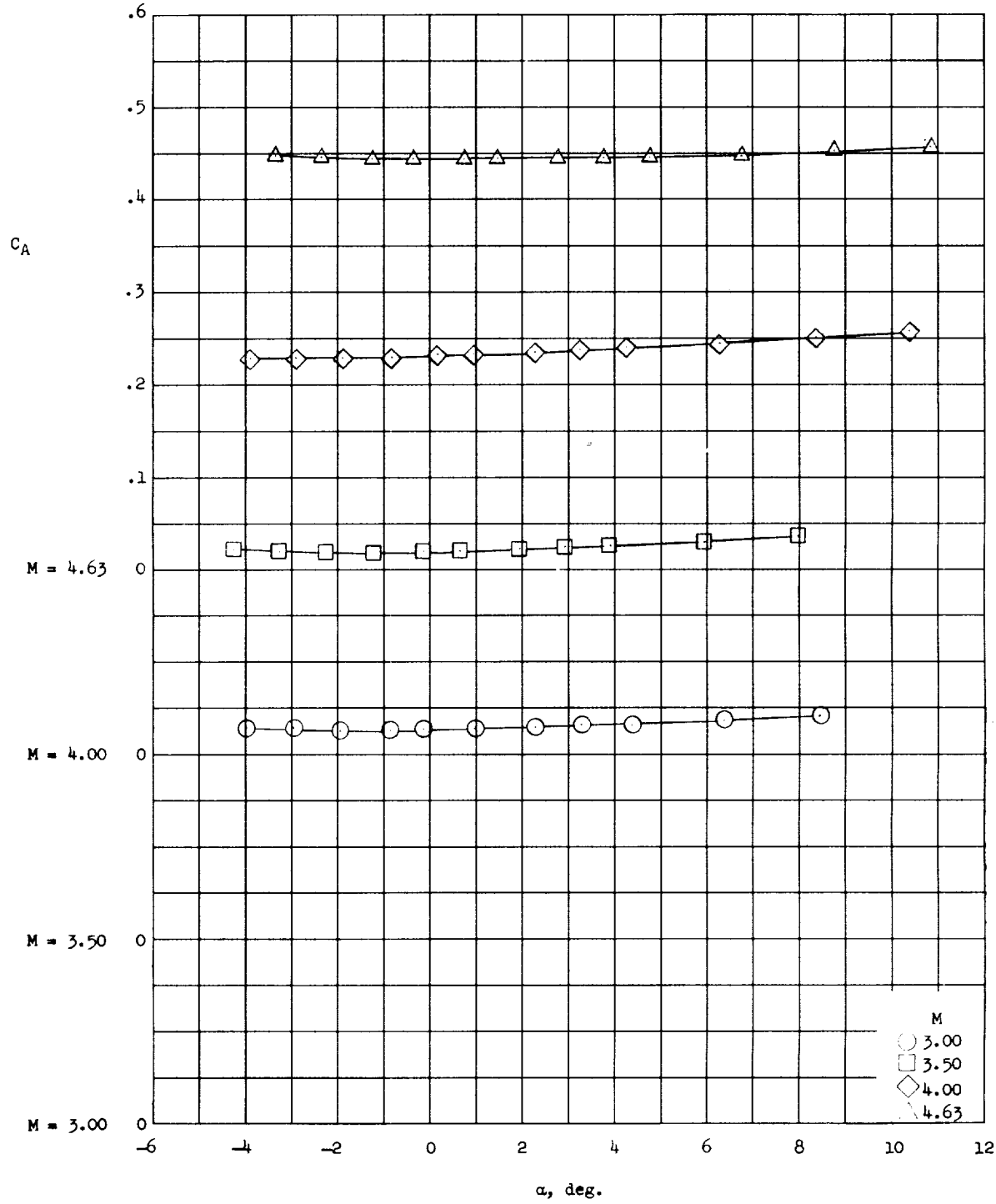

(b) C_A.

Figure 6.- Continued.

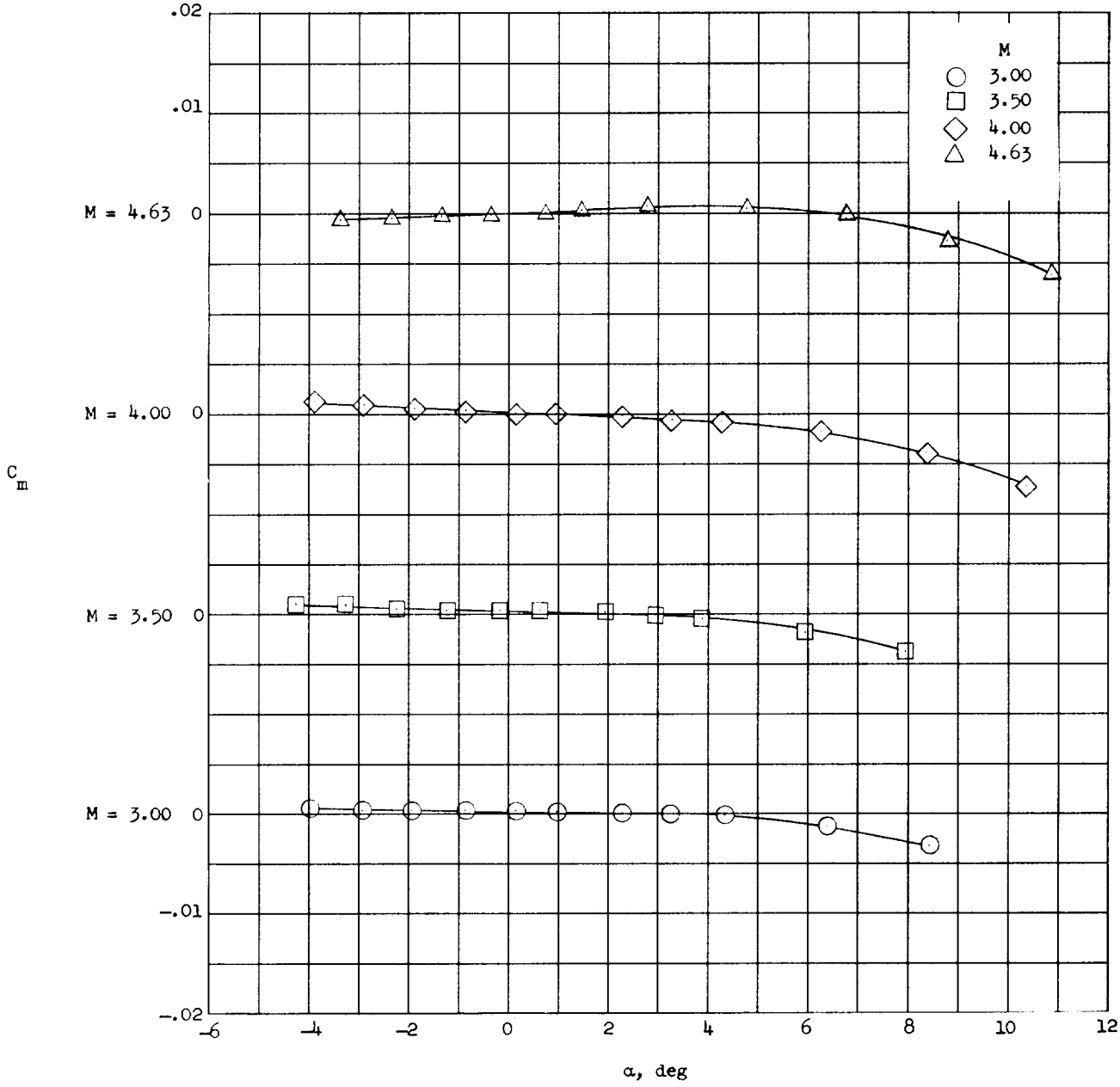

(c) C_m.

Figure 6.- Concluded.

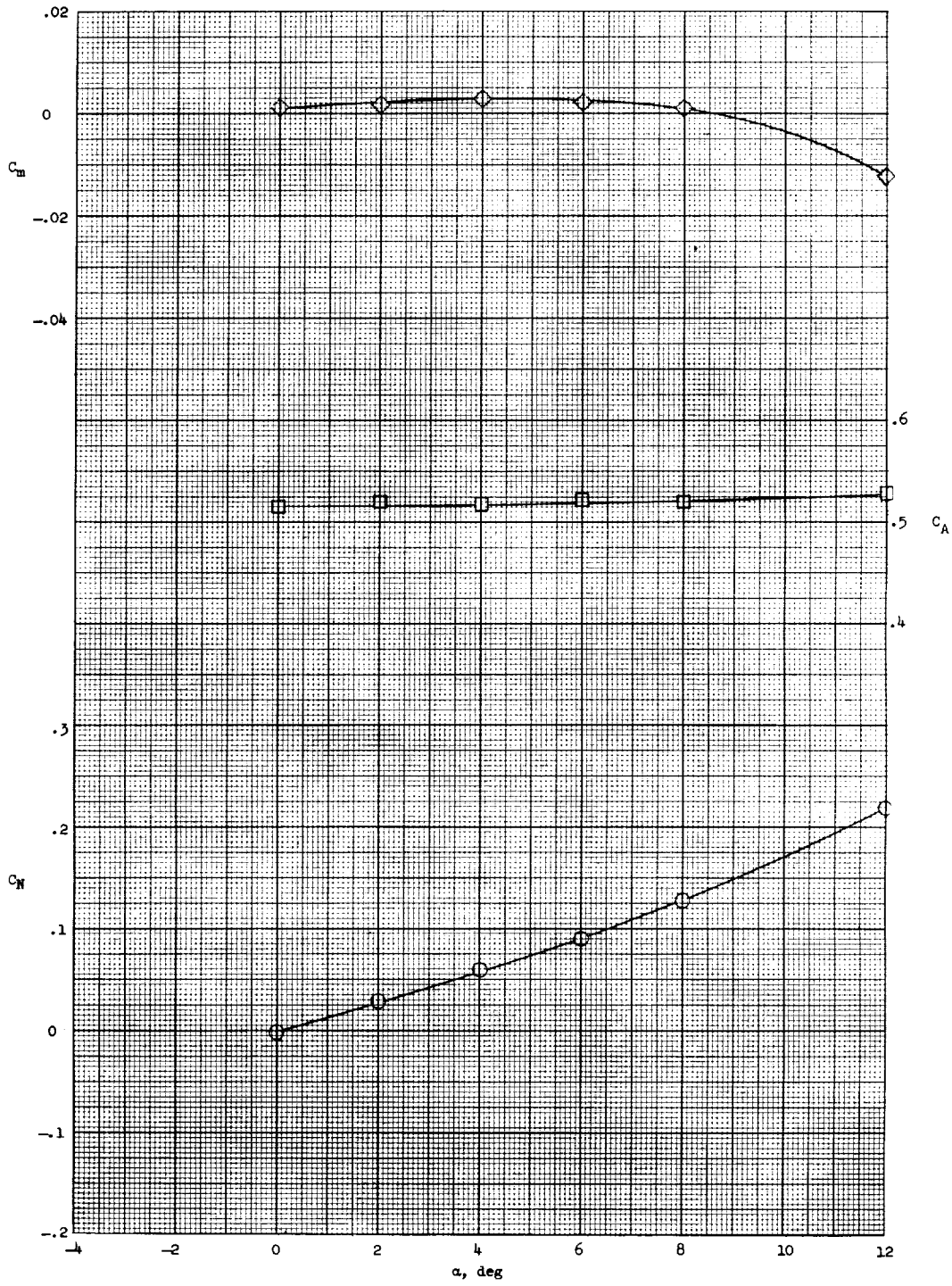

(a) N_1B_1.

Figure 7.- Longitudinal stability results on several configurations at M = 6.8.

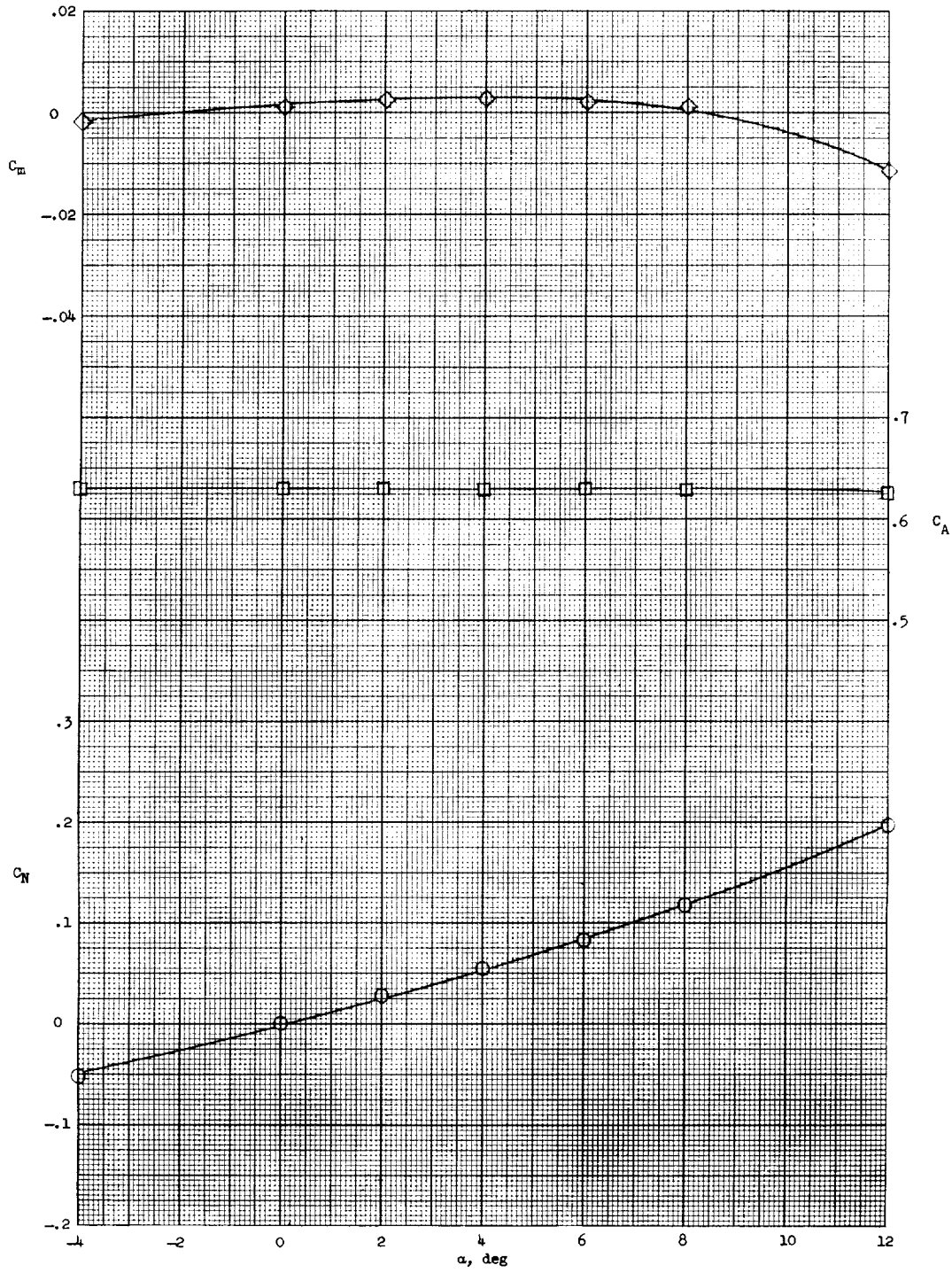

(b) N_2B_1.

Figure 7.- Continued.

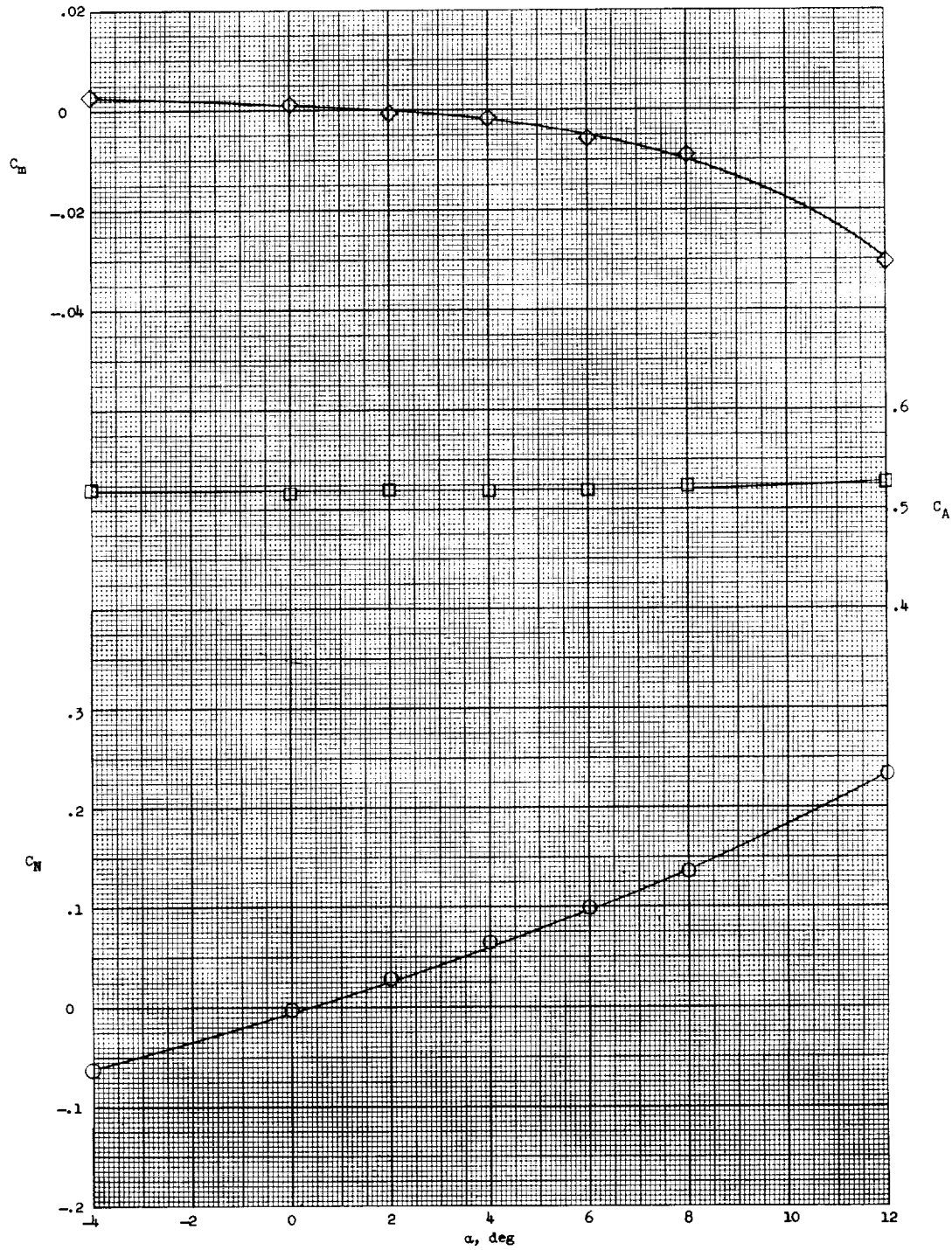

(c) N_1B_2.

Figure 7.- Continued.

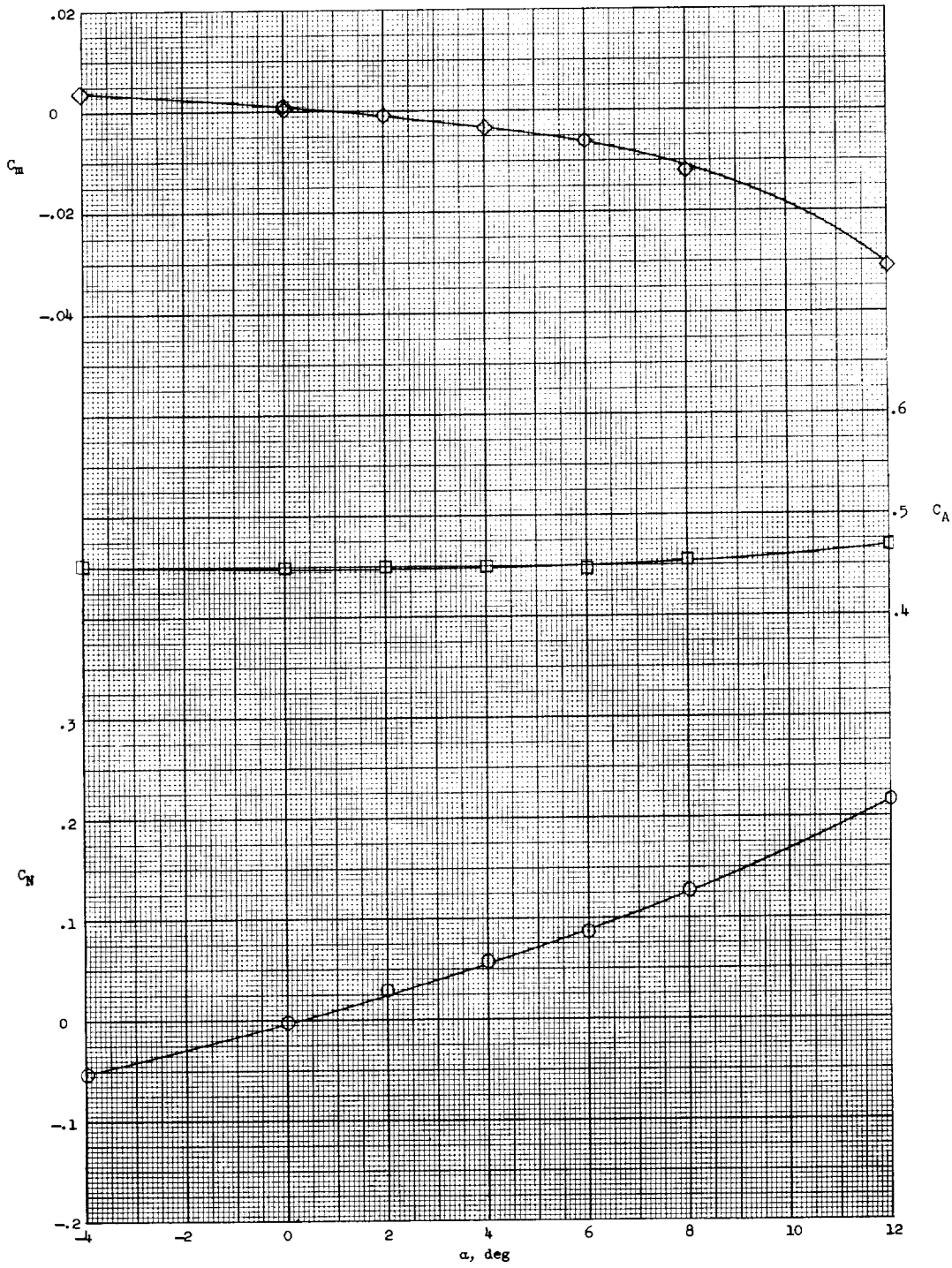

(d) N_1B_3.

Figure 7.- Continued.

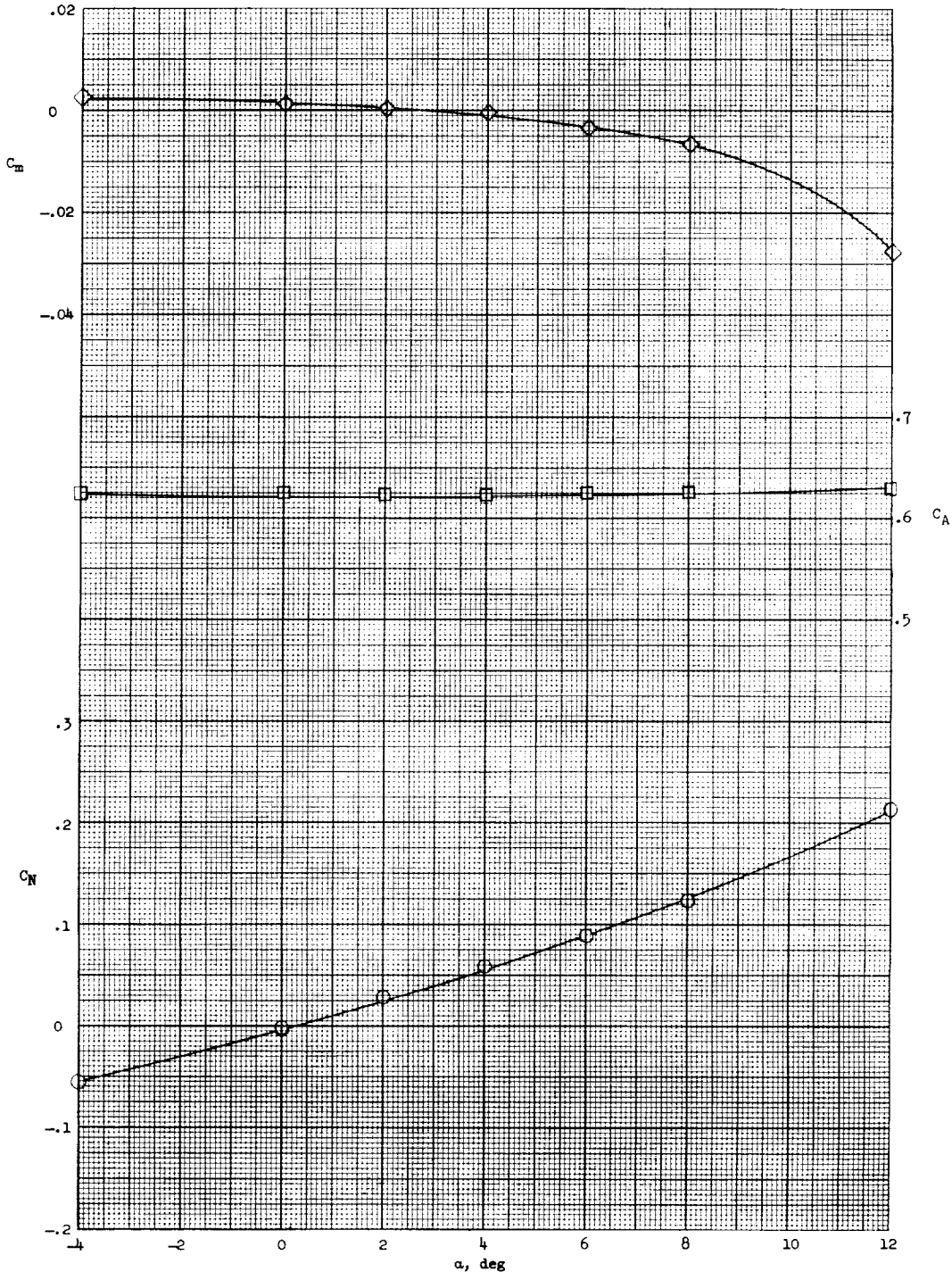

(e) N_2B_2.

Figure 7.- Continued.

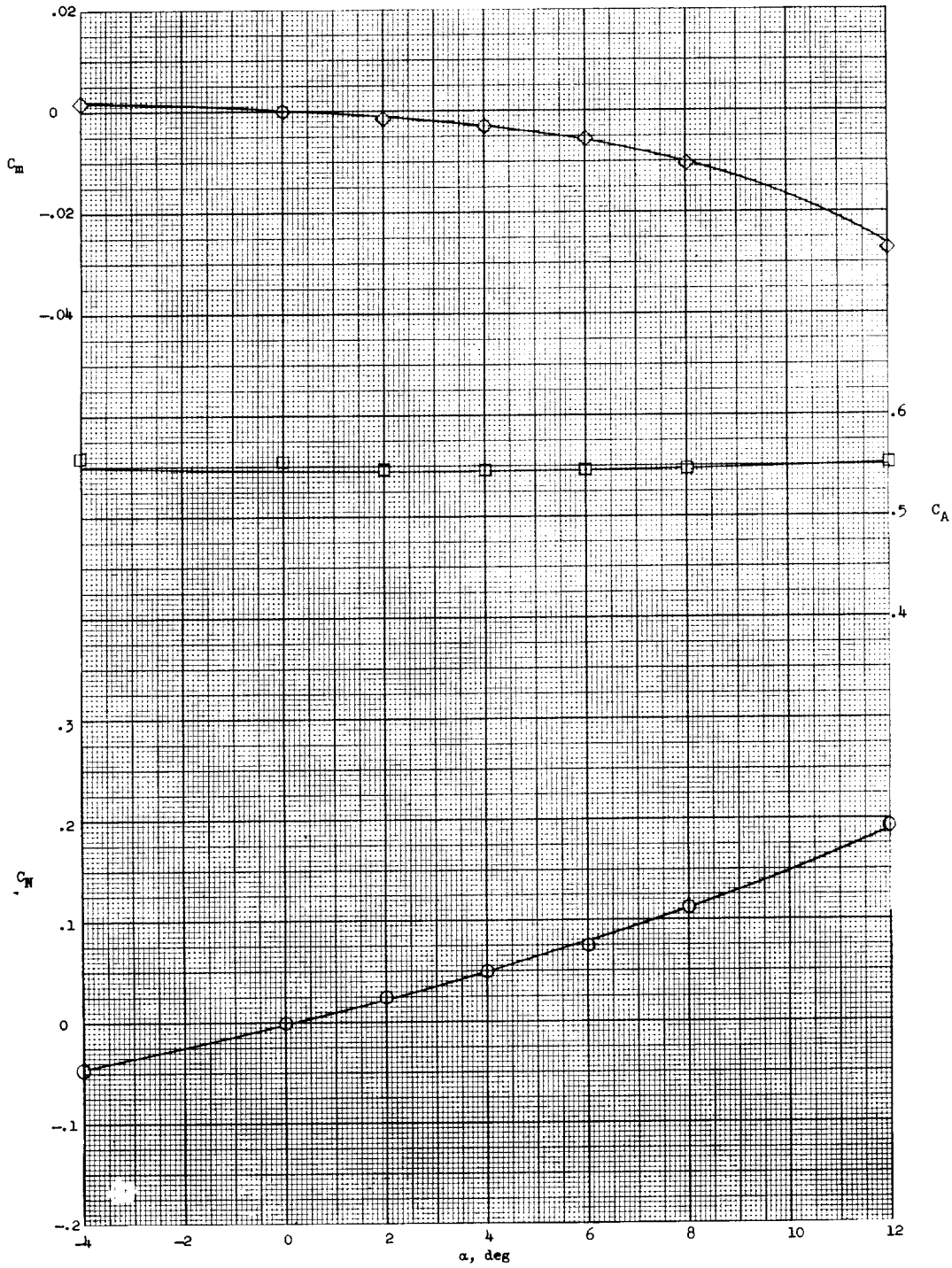

(f) N_2B_5.

Figure 7.- Continued.

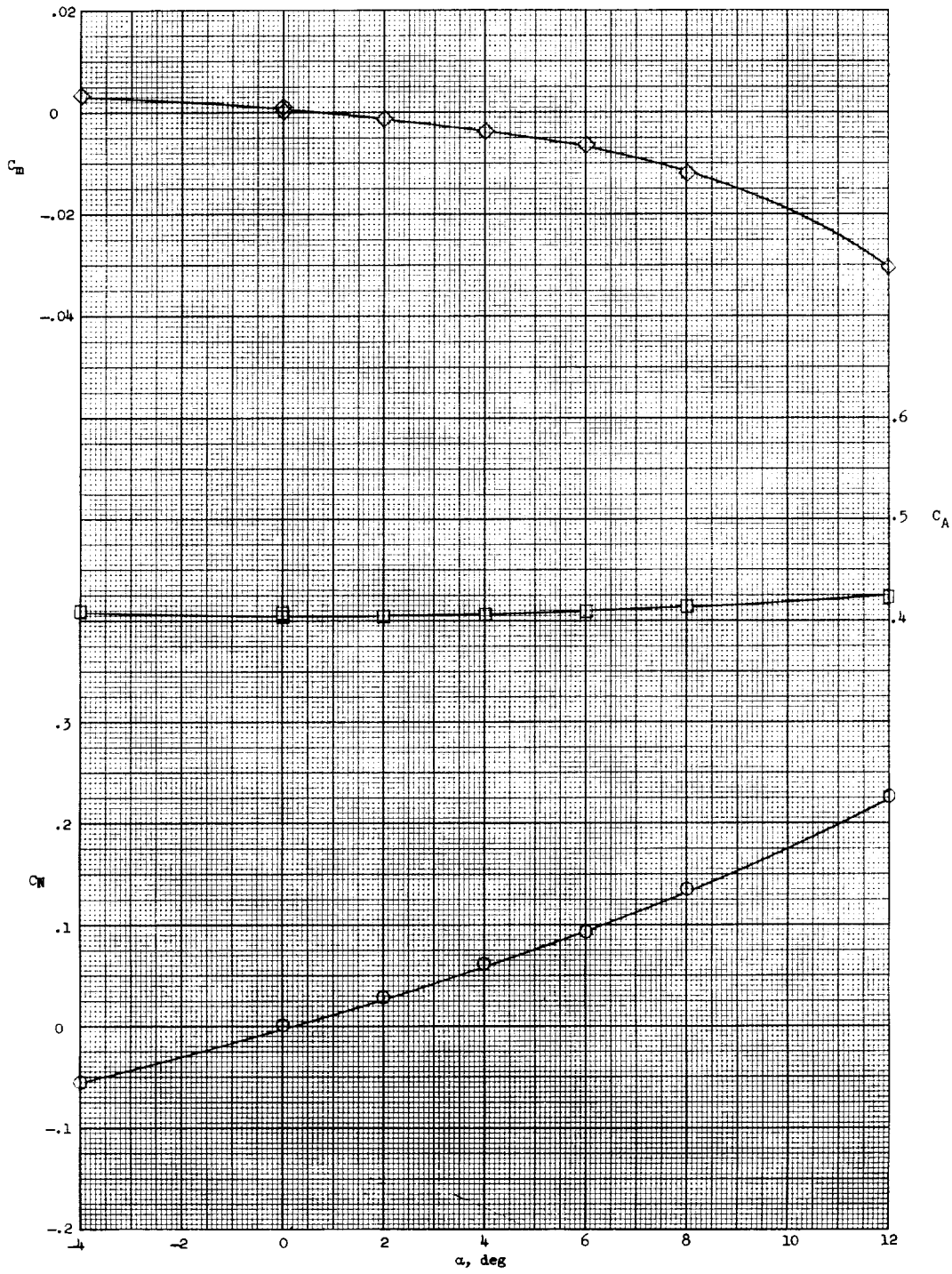

(g) N_3B_3.

Figure 7.- Concluded.

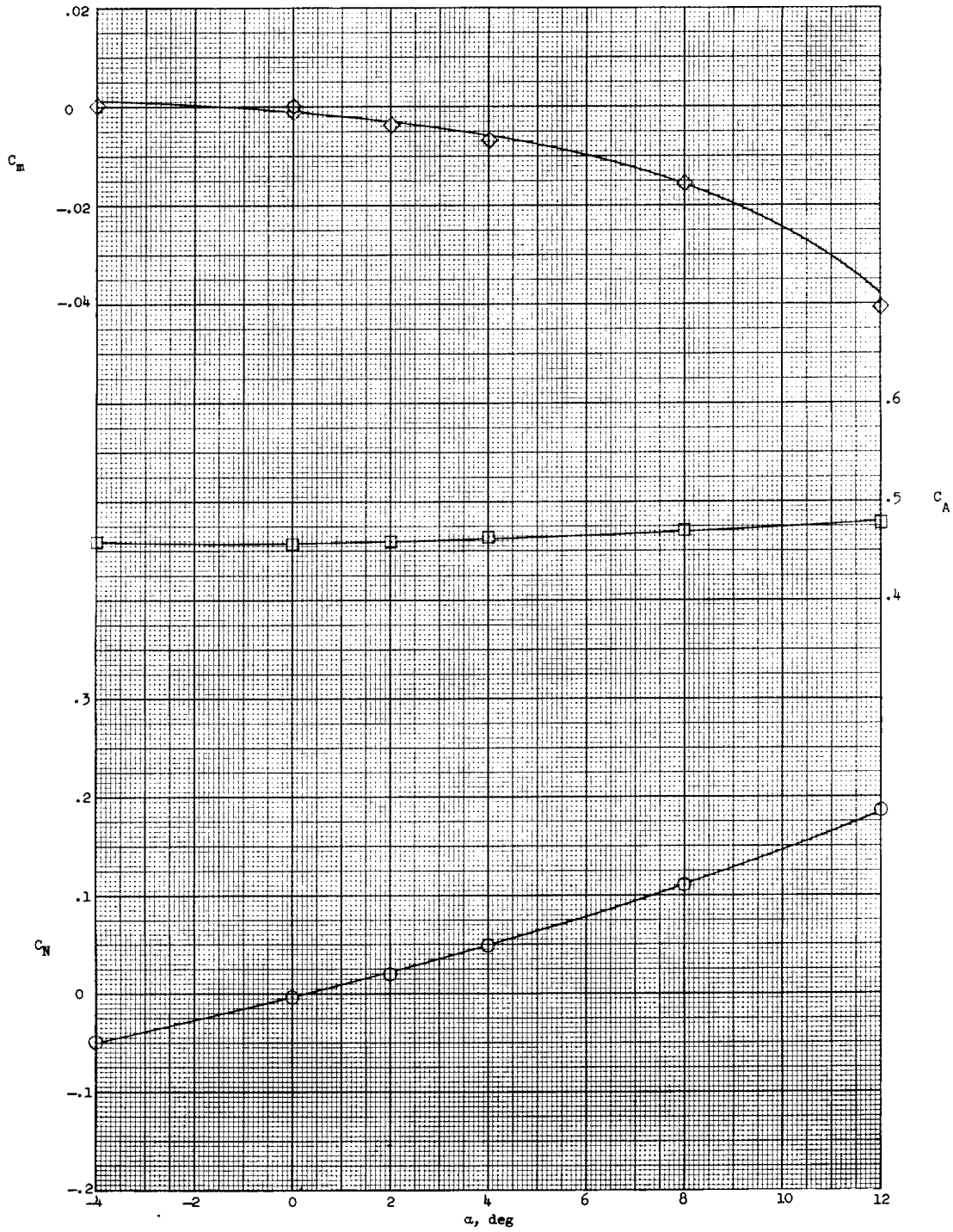

(a) N_1B_3.

Figure 8.- Longitudinal stability results on several configurations at M = 9.6.

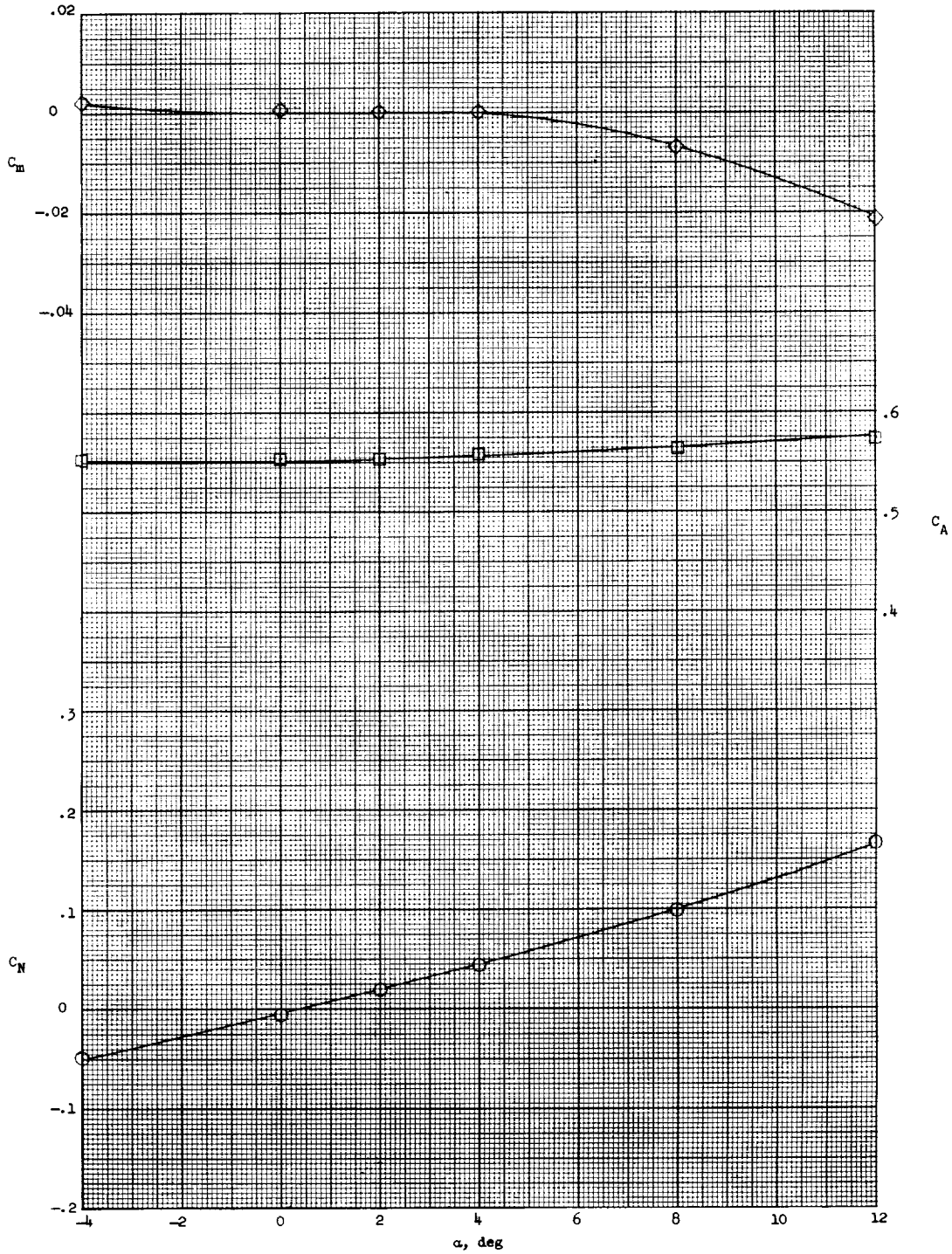

(b) N_2B_3.

Figure 8.- Continued.

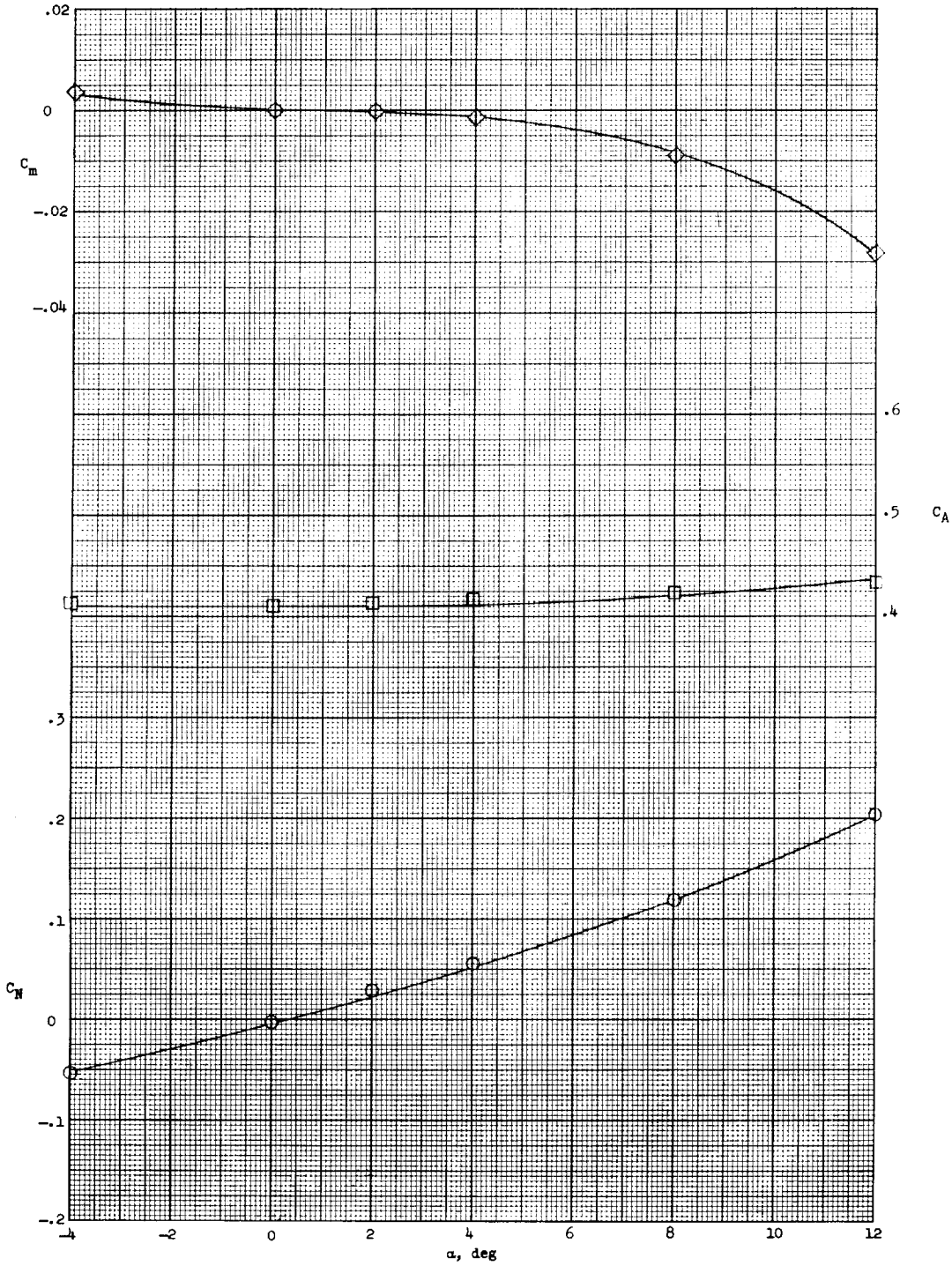

(c) N_3B_3.

Figure 8.- Concluded.

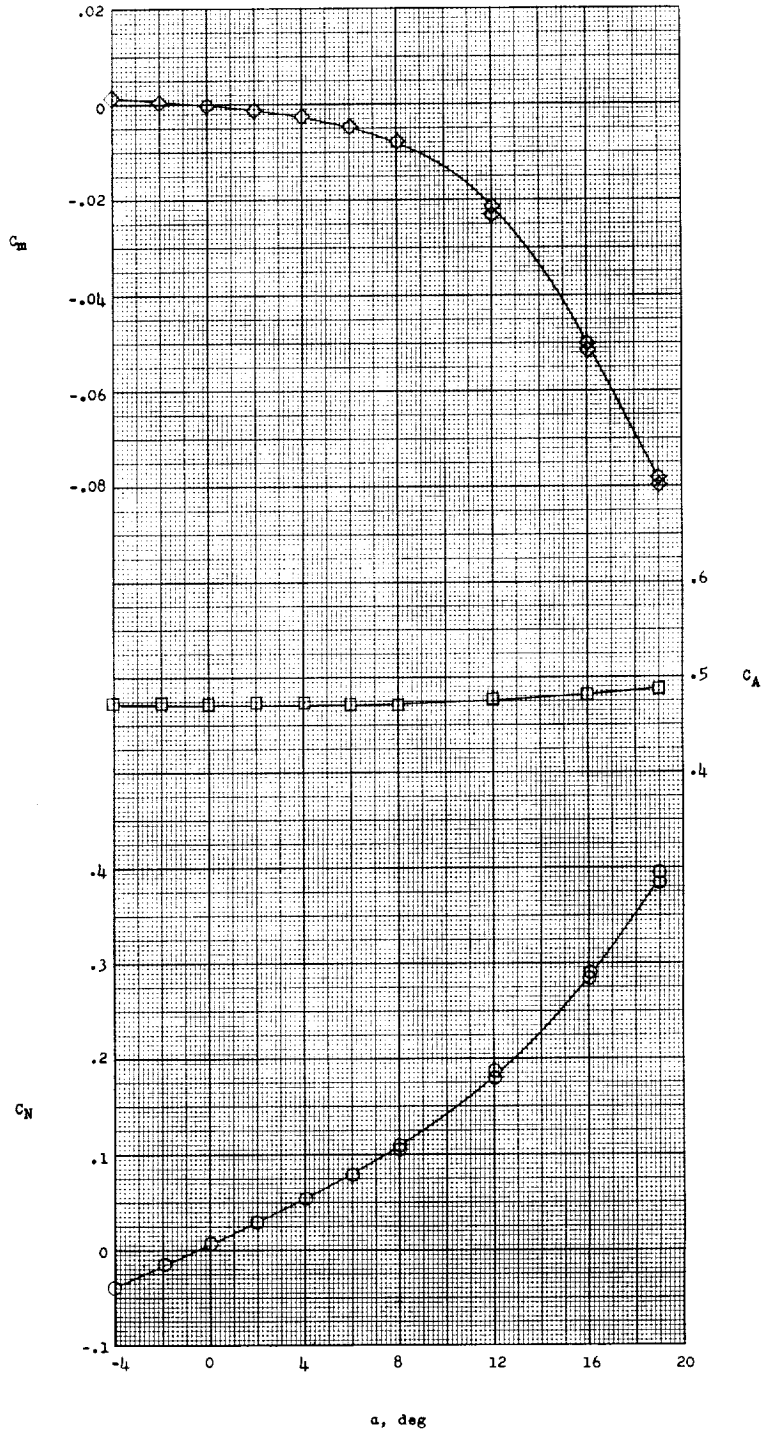

(a) N_1B_3.

Figure 9.- Longitudinal stability results on several configurations at M = 24.4.

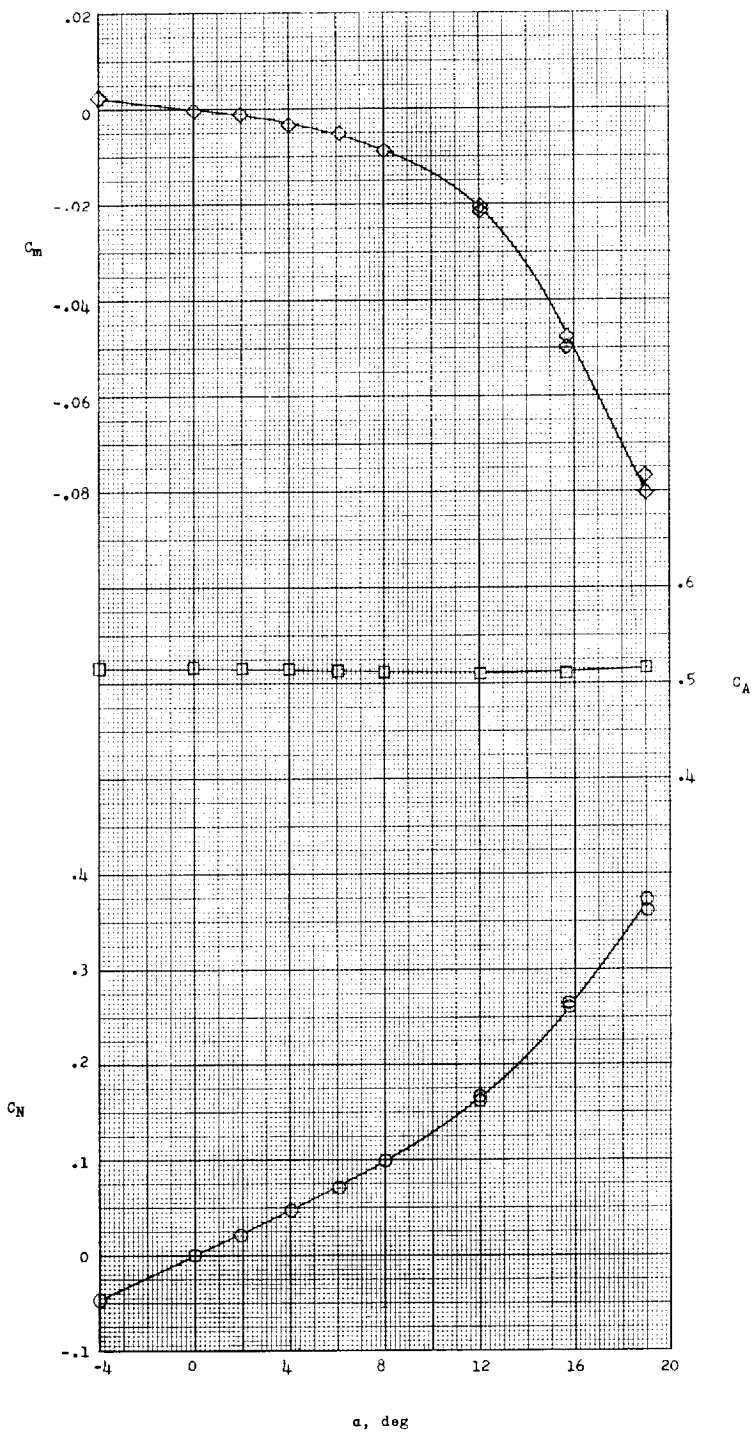

(b) $N_{1S}B_3$.

Figure 9.- Continued.

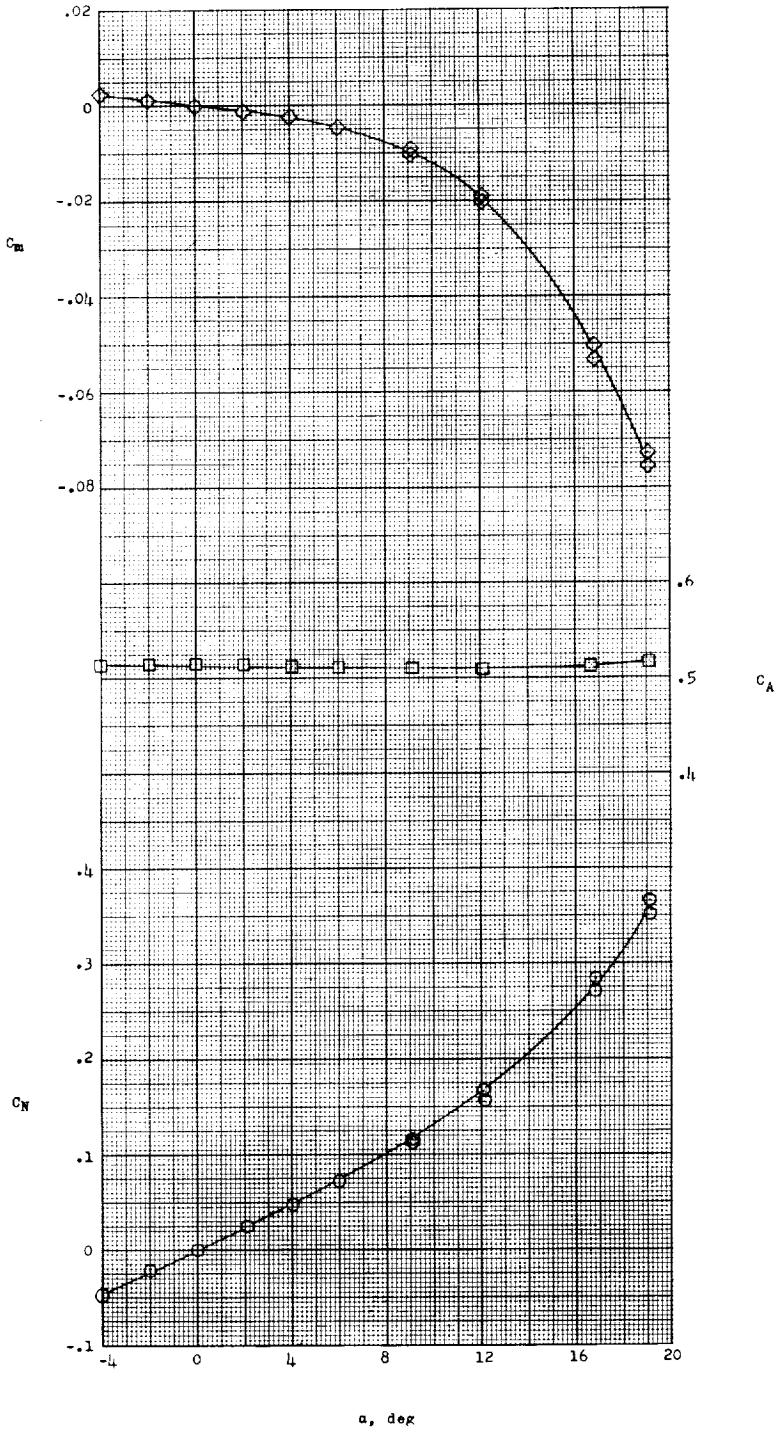

(c) N_4B_4.

Figure 9.- Continued.

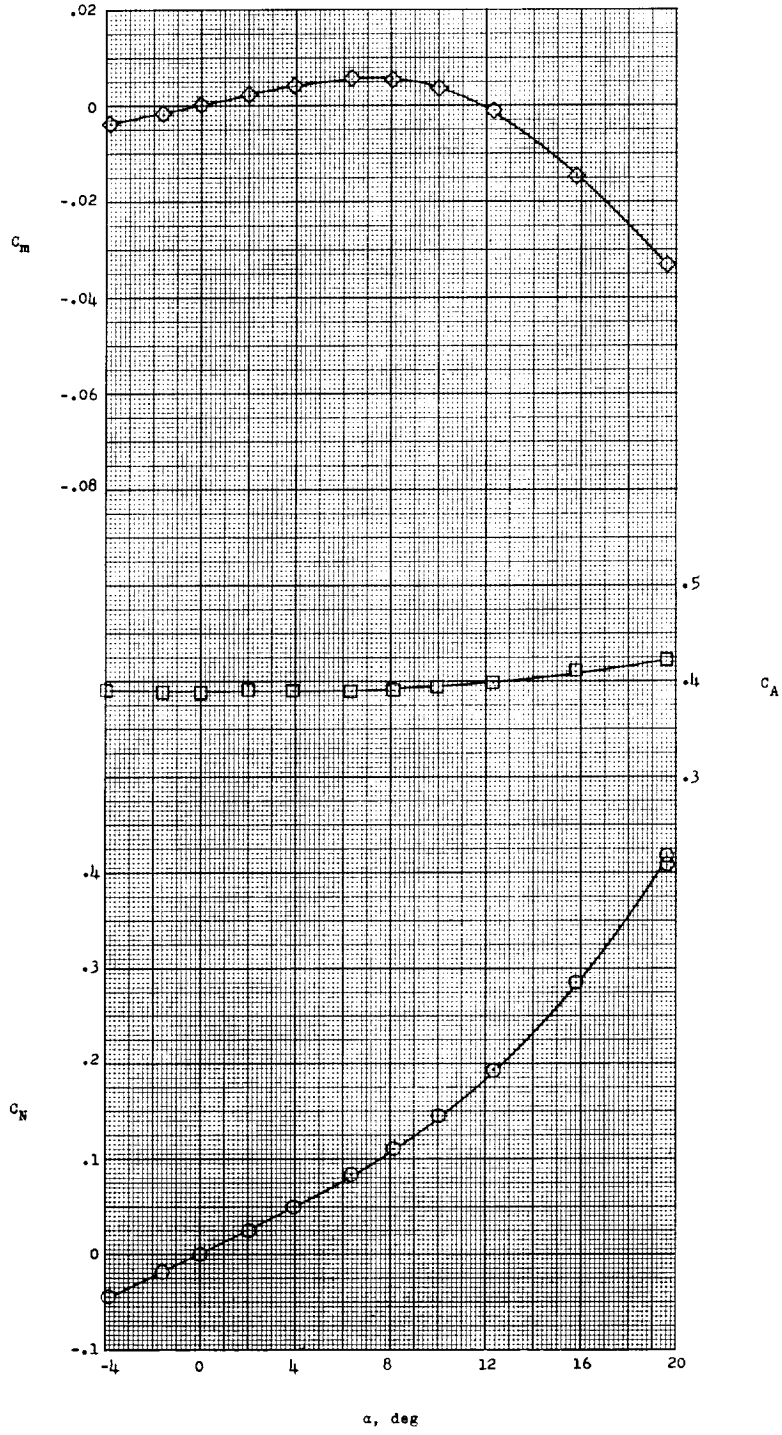

(d) N_5B_5.

Figure 9.- Continued.

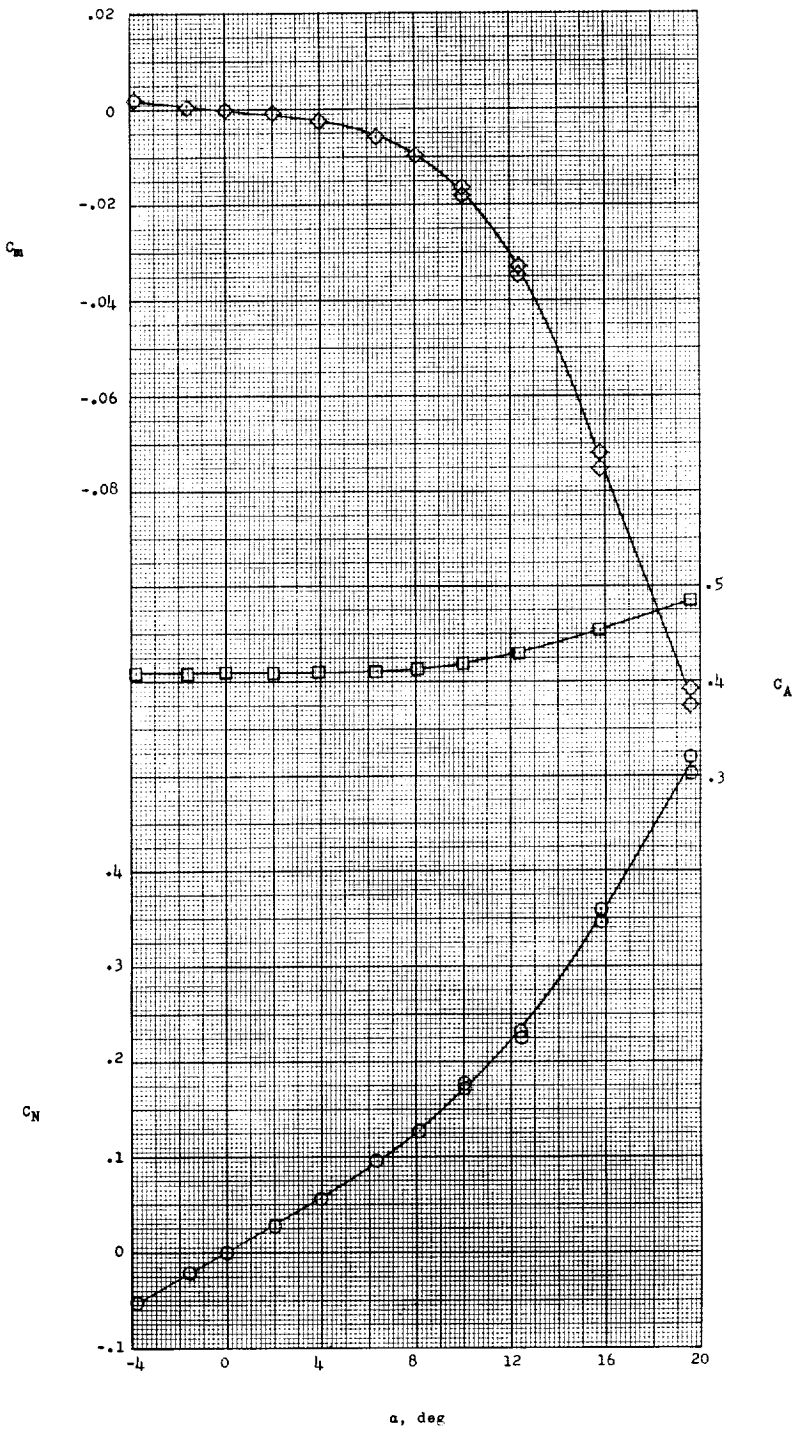

(e) $N_5B_5F_1$.

Figure 9.- Continued.

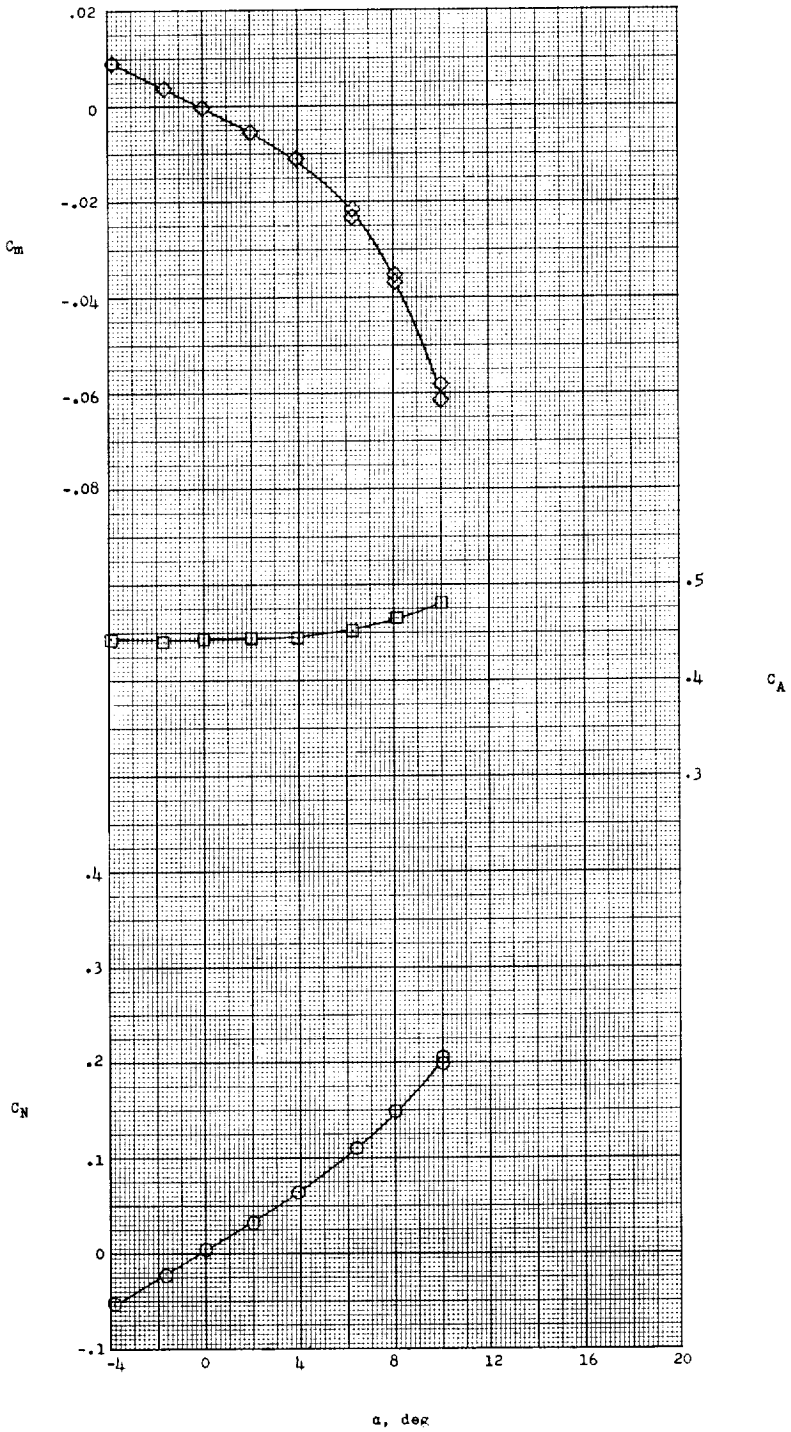

(f) $N_5B_5F_2$.

Figure 9.- Concluded.

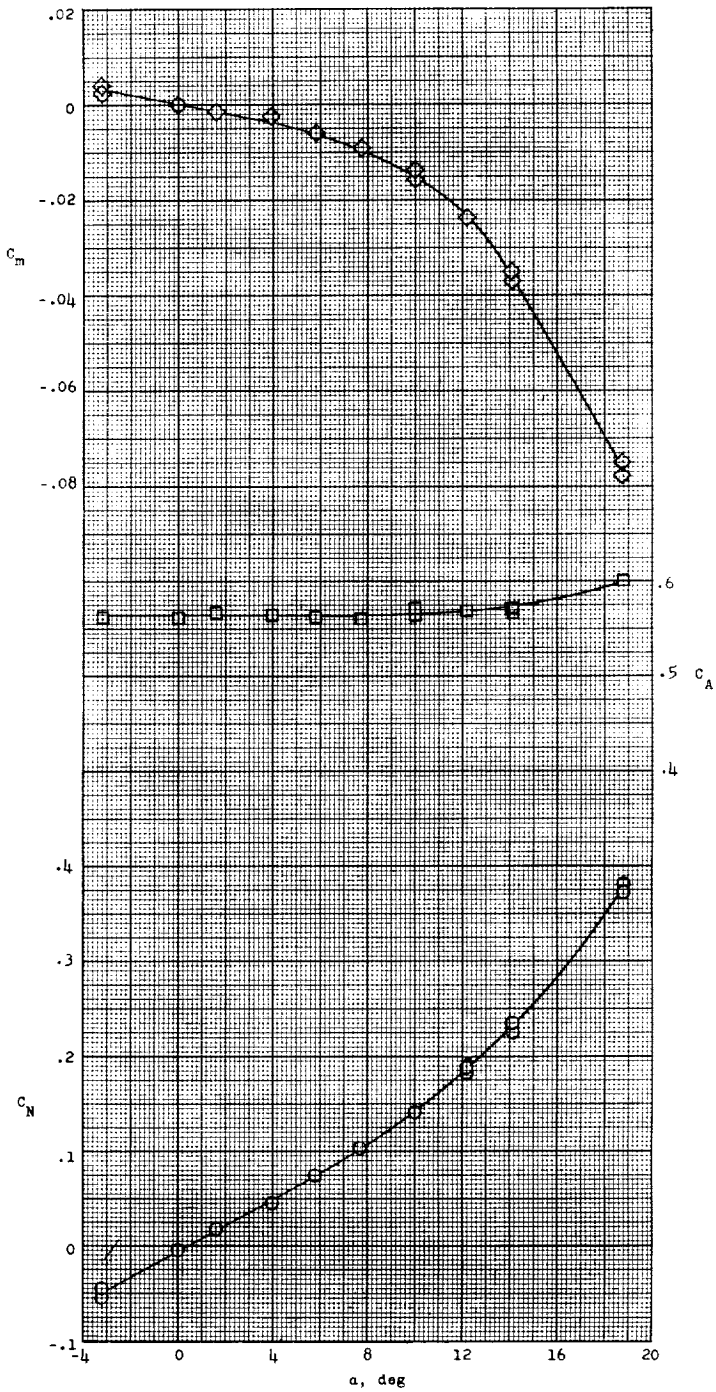

(a) M = 20.2; $R_D = 0.48 \times 10^6$.

Figure 10.- Longitudinal stability of configuration N_4B_4 at several values of R_D.

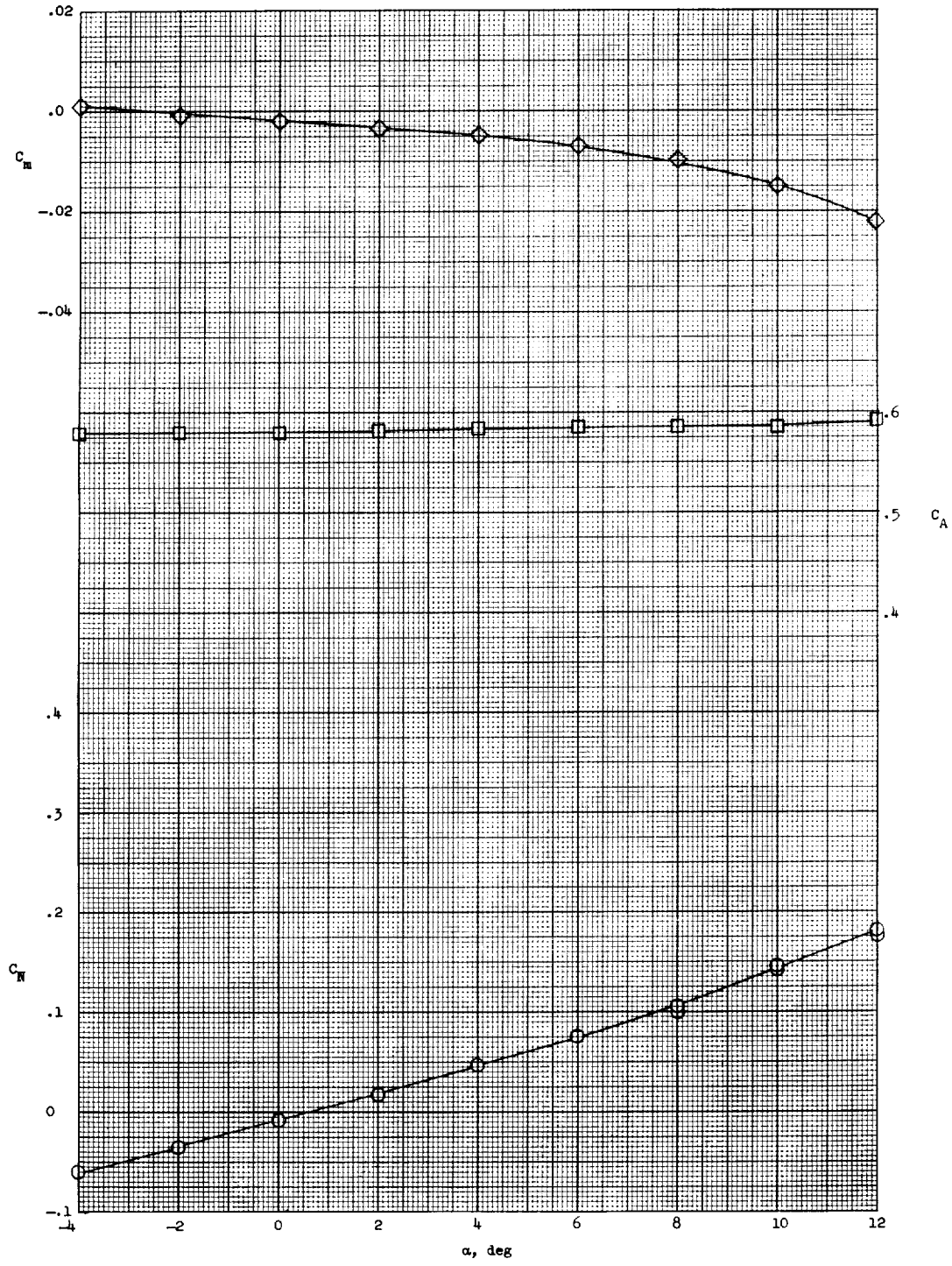

(b) M = 20.2; $R_D = 0.96 \times 10^6$.

Figure 10.- Continued.

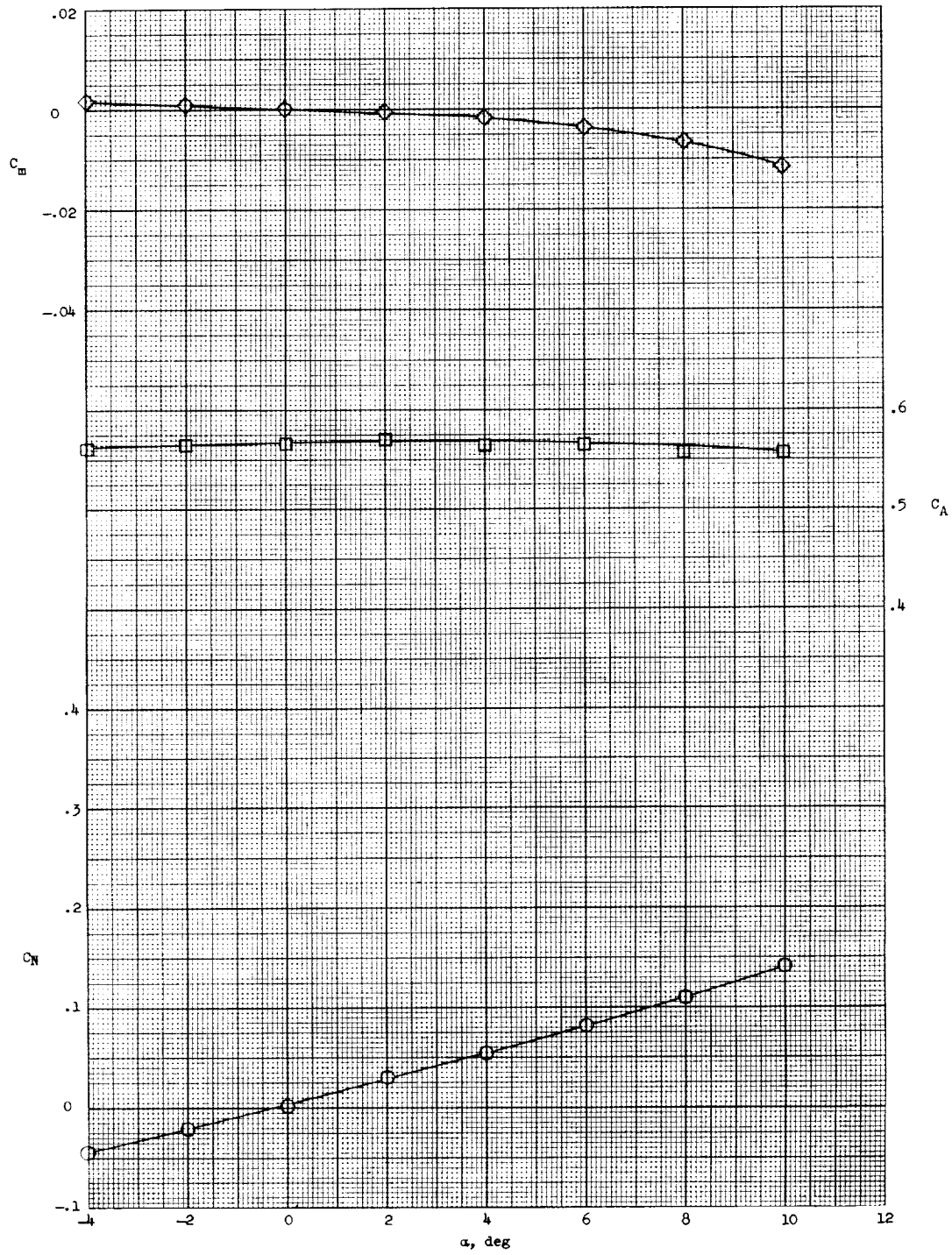

(c) M = 20.2; $R_D = 1.93 \times 10^6$.

Figure 10.- Continued.

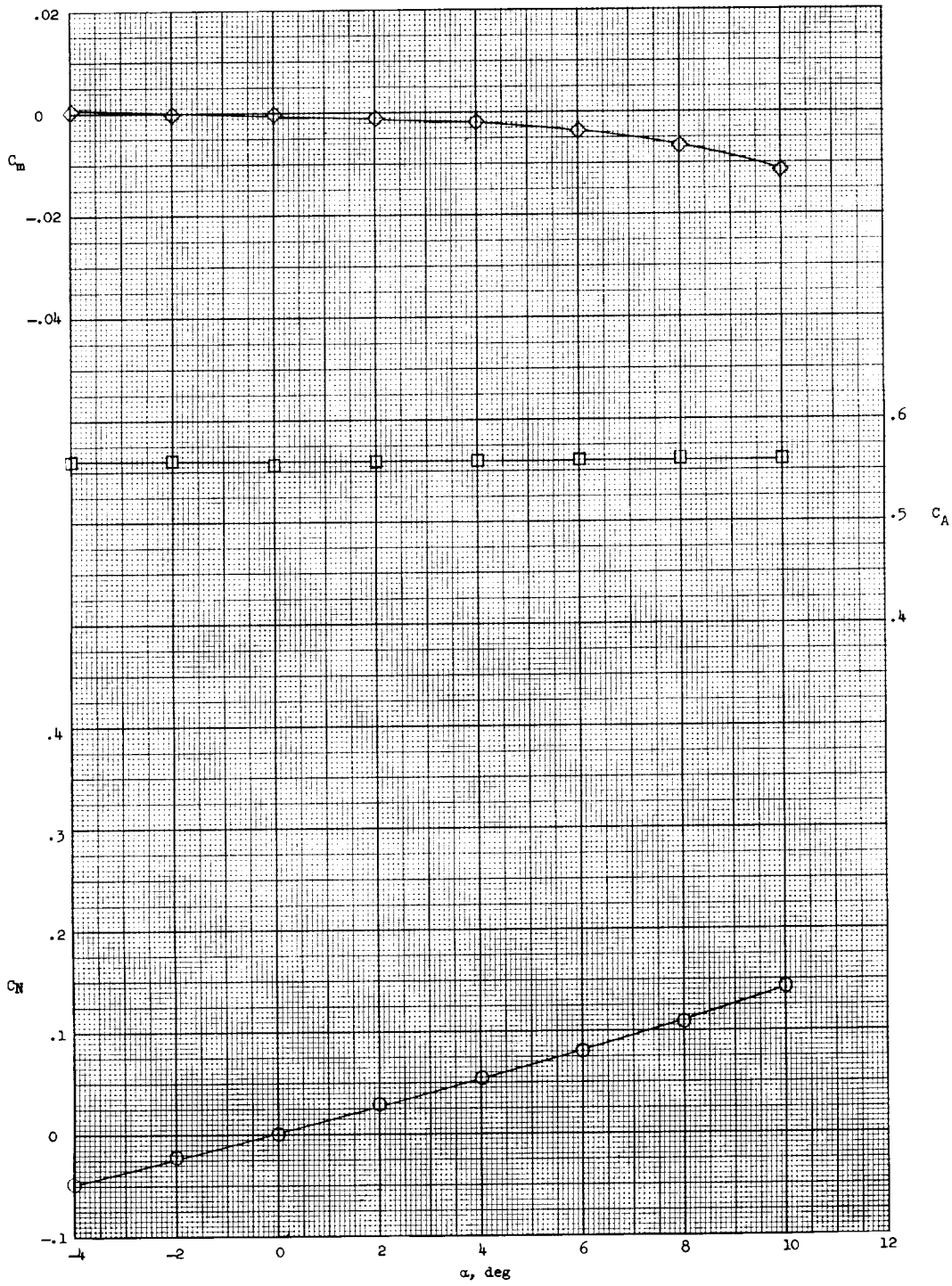

(d) M = 21.2; $R_D = 3.50 \times 10^6$.

Figure 10.- Concluded.

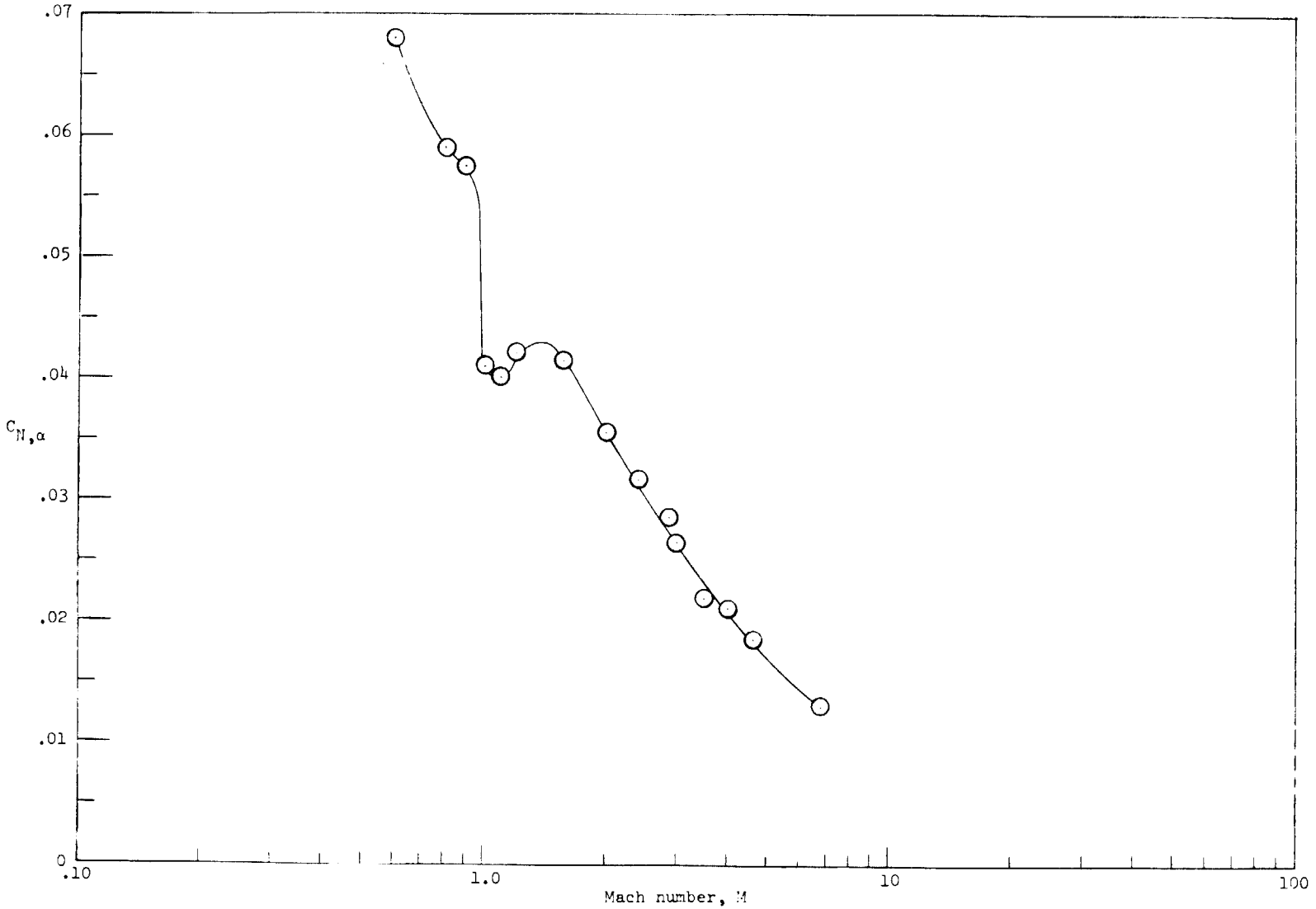

(a) $C_{N,\alpha}$.

Figure 11.- Effect of Mach number on the stability of configuration N_1B_1 at $\alpha = 0^\circ$.

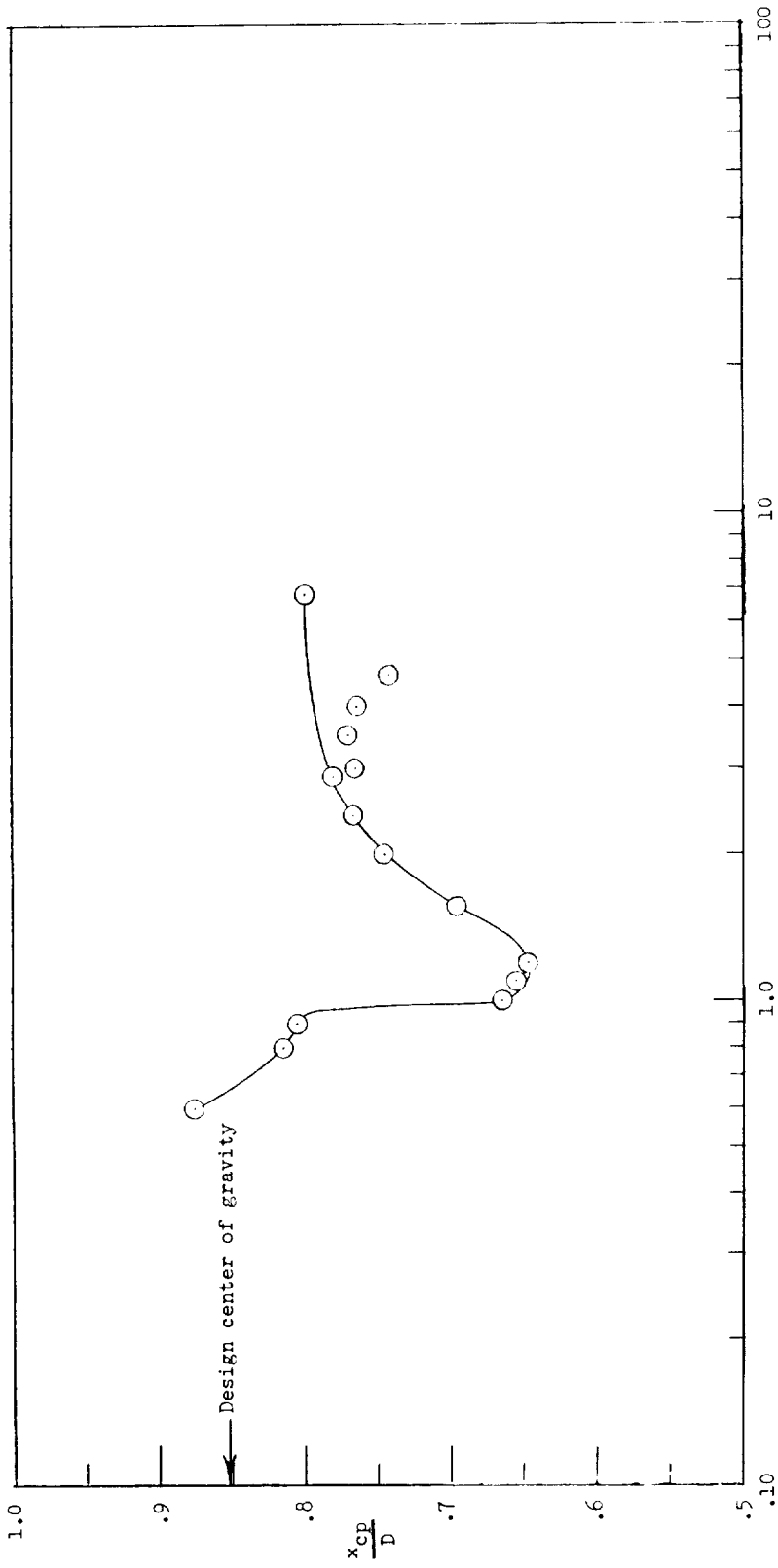

(b) $\frac{x_{cp}}{D}$.

Figure 11.- Concluded.

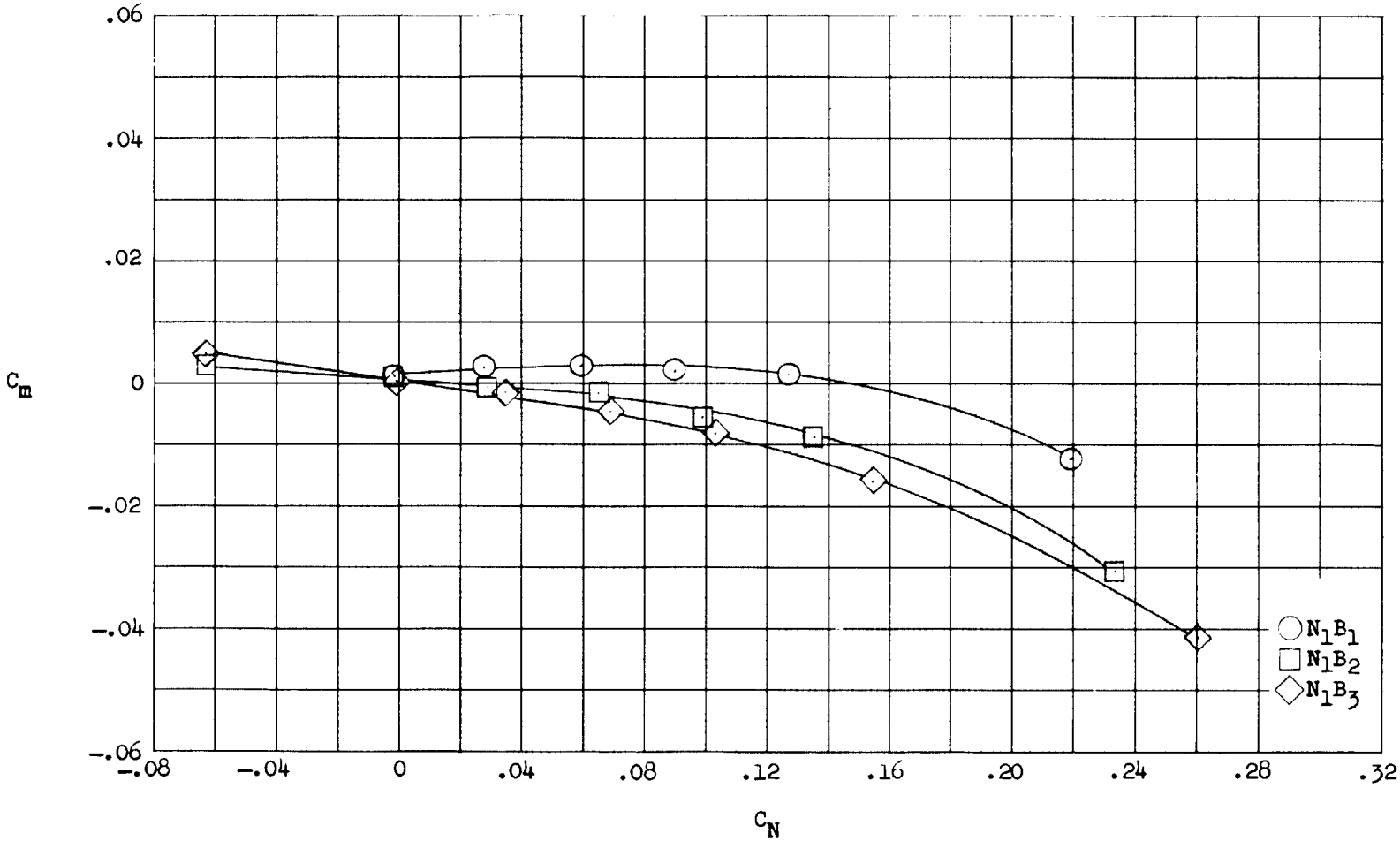

Figure 12.- The effect of body shape on the stability at M = 6.8. (Reference diameter equal to that of configuration N_1B_1)

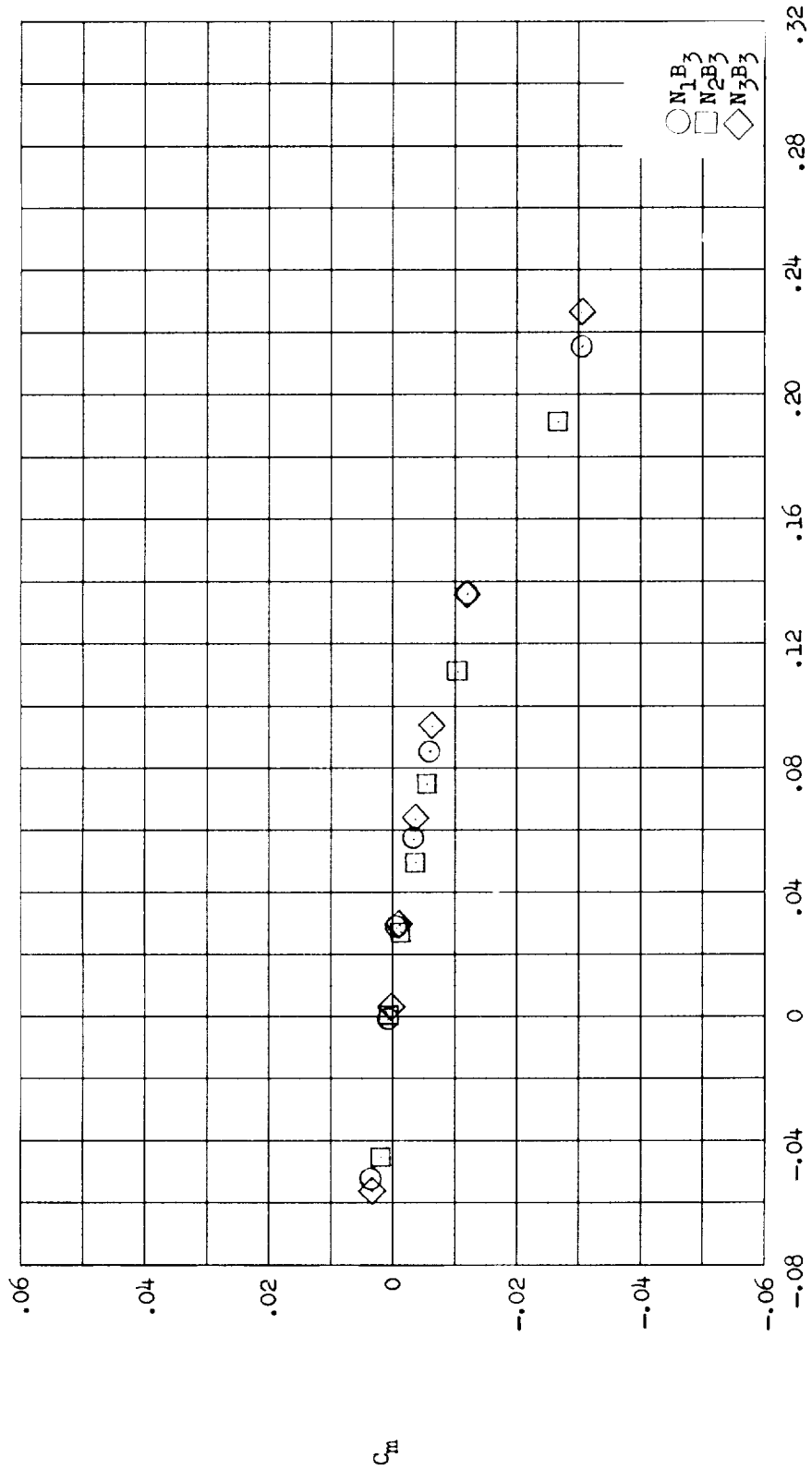

Figure 13.- The effect of nose shape on the longitudinal stability at M = 6.8.

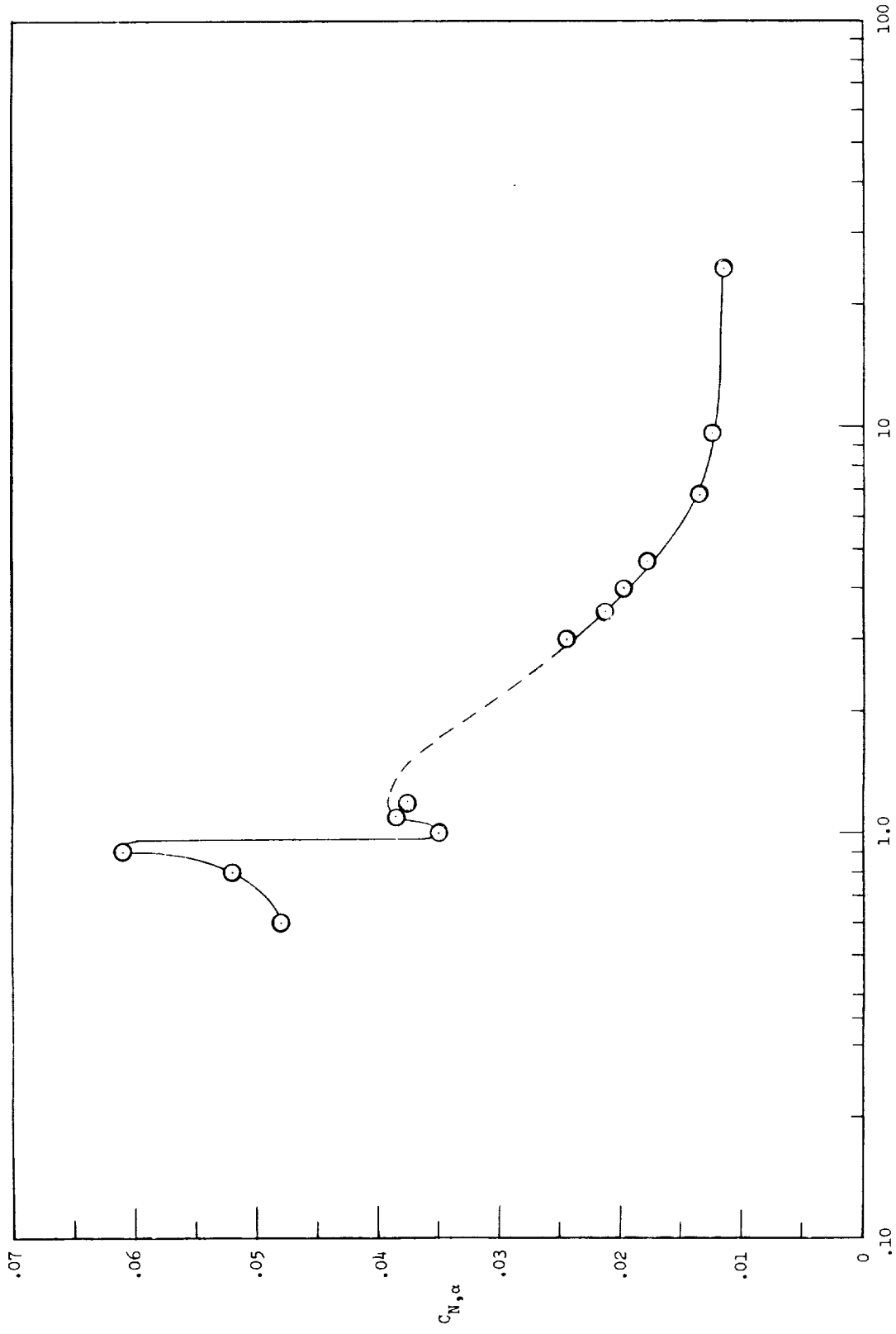

(a) $C_{N,\alpha}$.

Figure 14.- Effect of Mach number on the stability of configuration N_1B_3 at $\alpha = 0^\circ$.

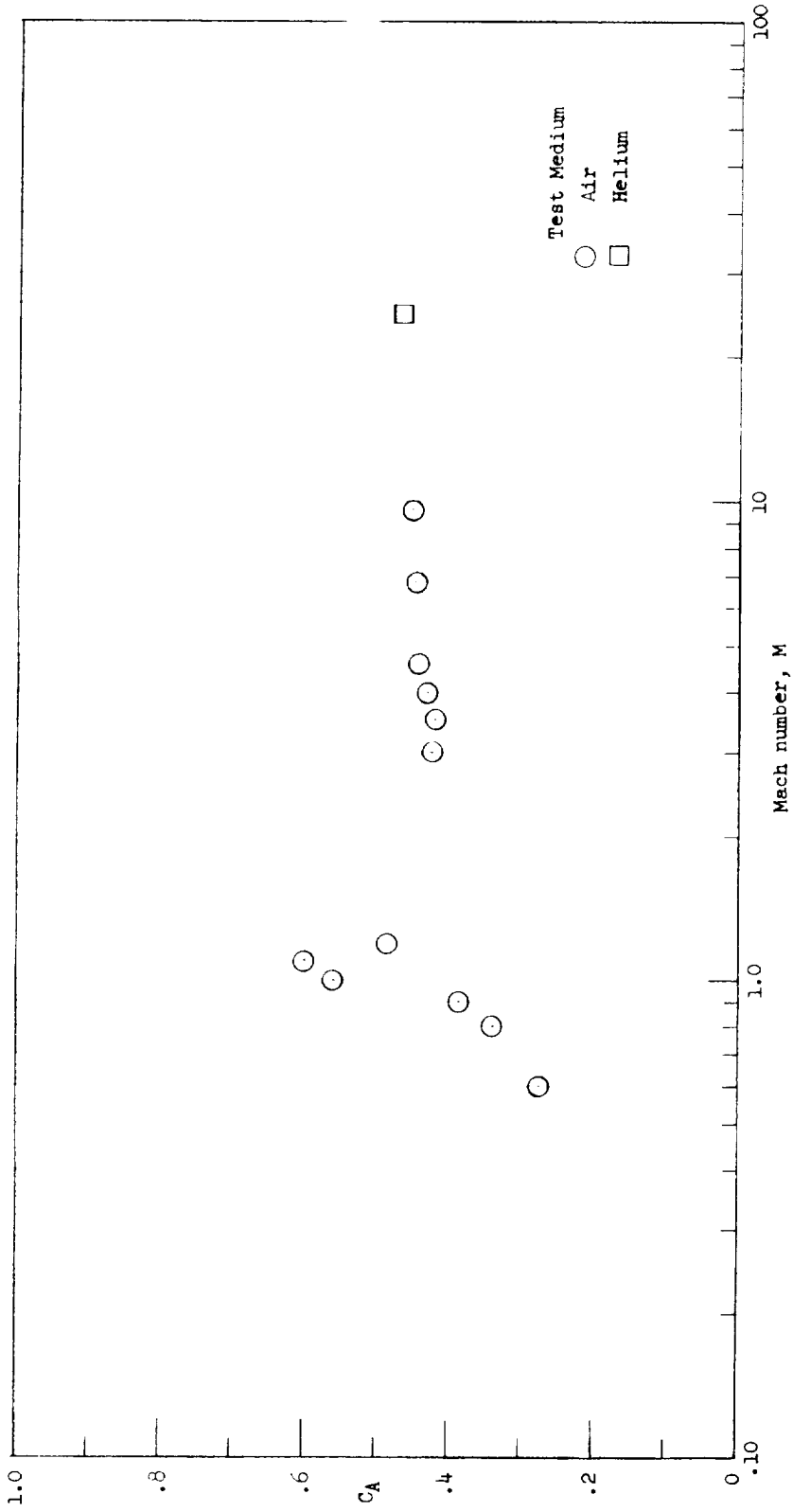

(b) C_A.

Figure 14.- Continued.

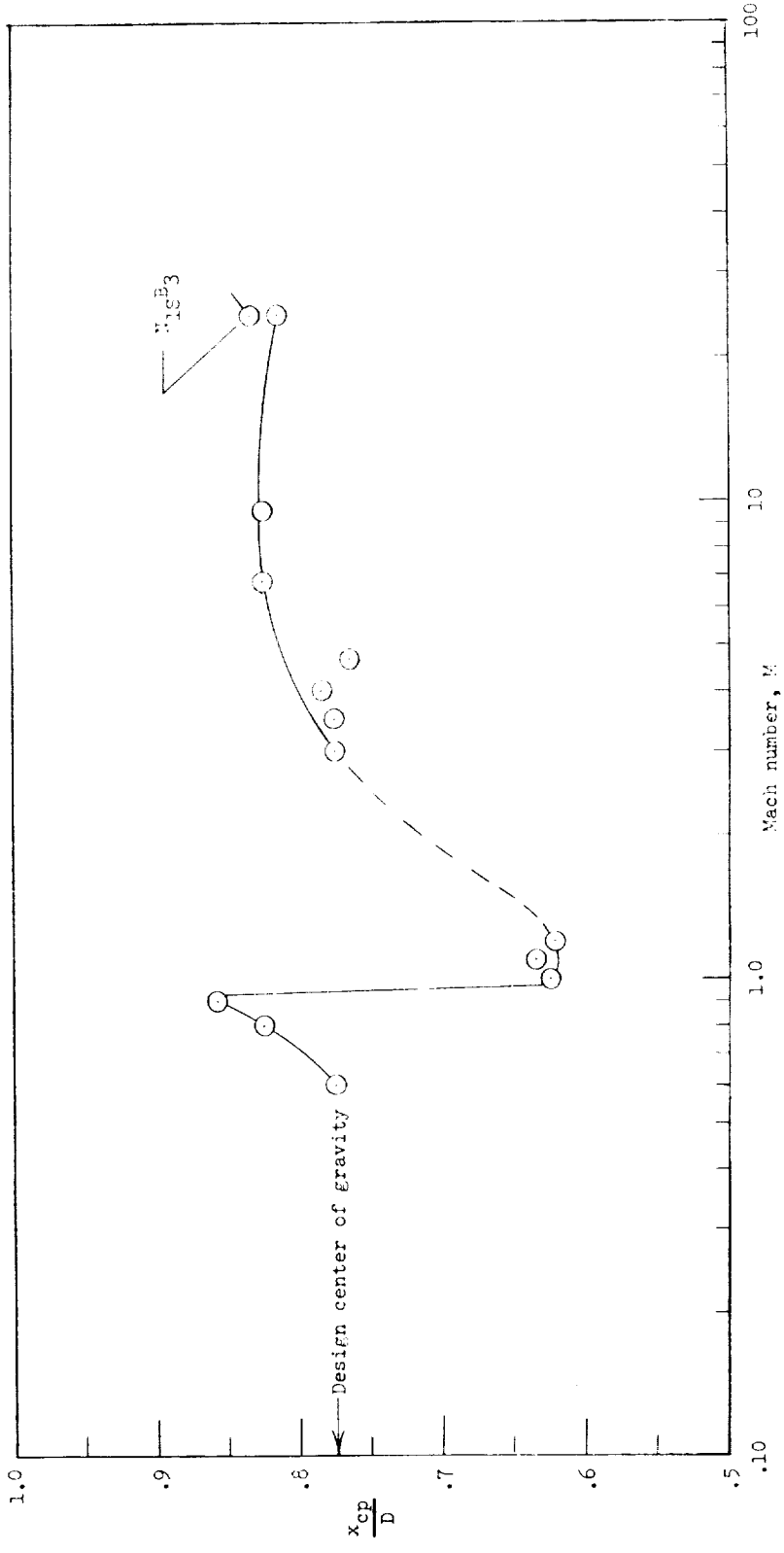

(c) $\frac{x_{cp}}{D}$.

Figure 14.- Concluded.

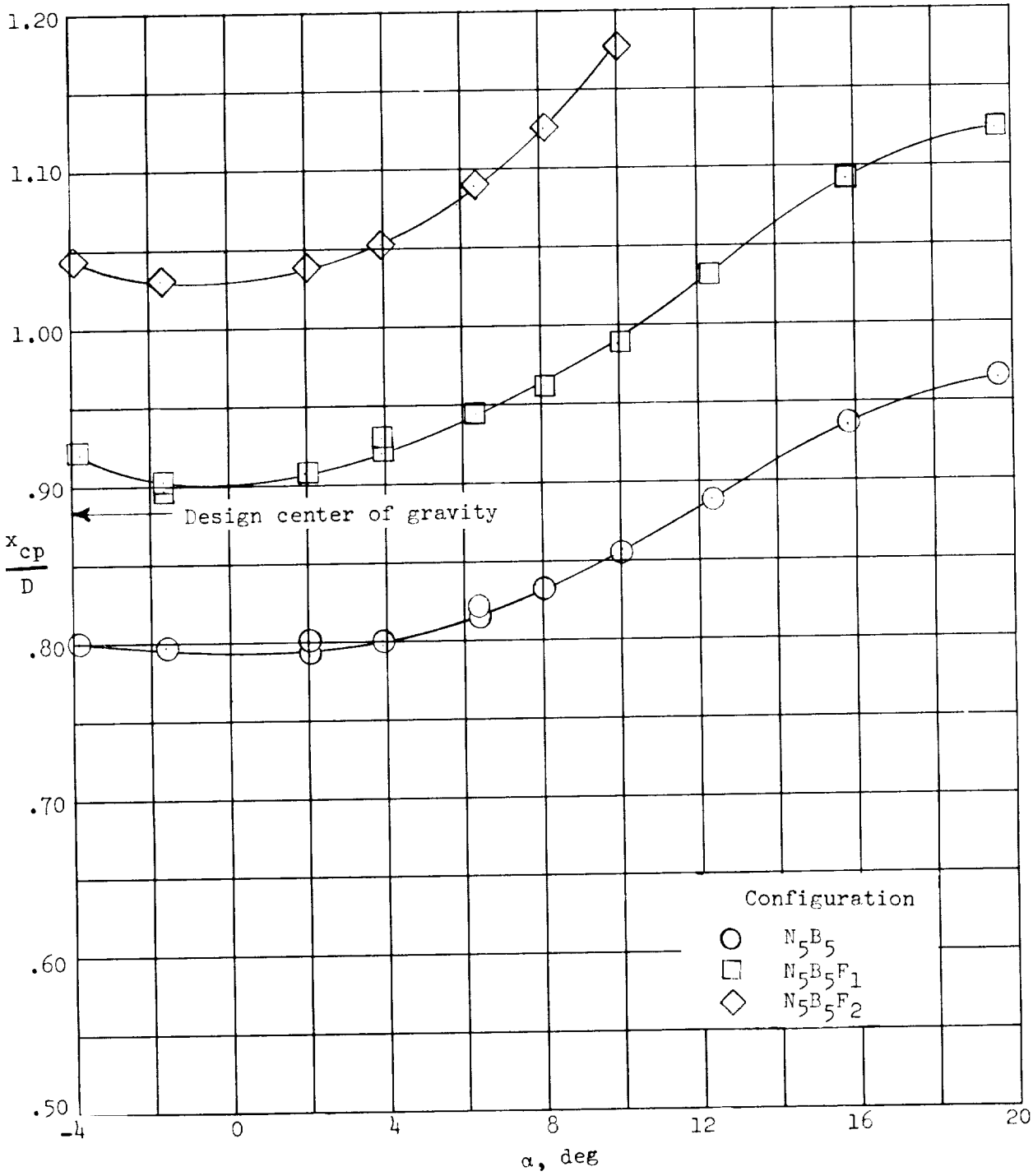

Figure 15.- The effect of adding a flare on the center of pressure of configuration N_5B_5. $M = 24.4$; $R_D = 0.71 \times 10^6$.

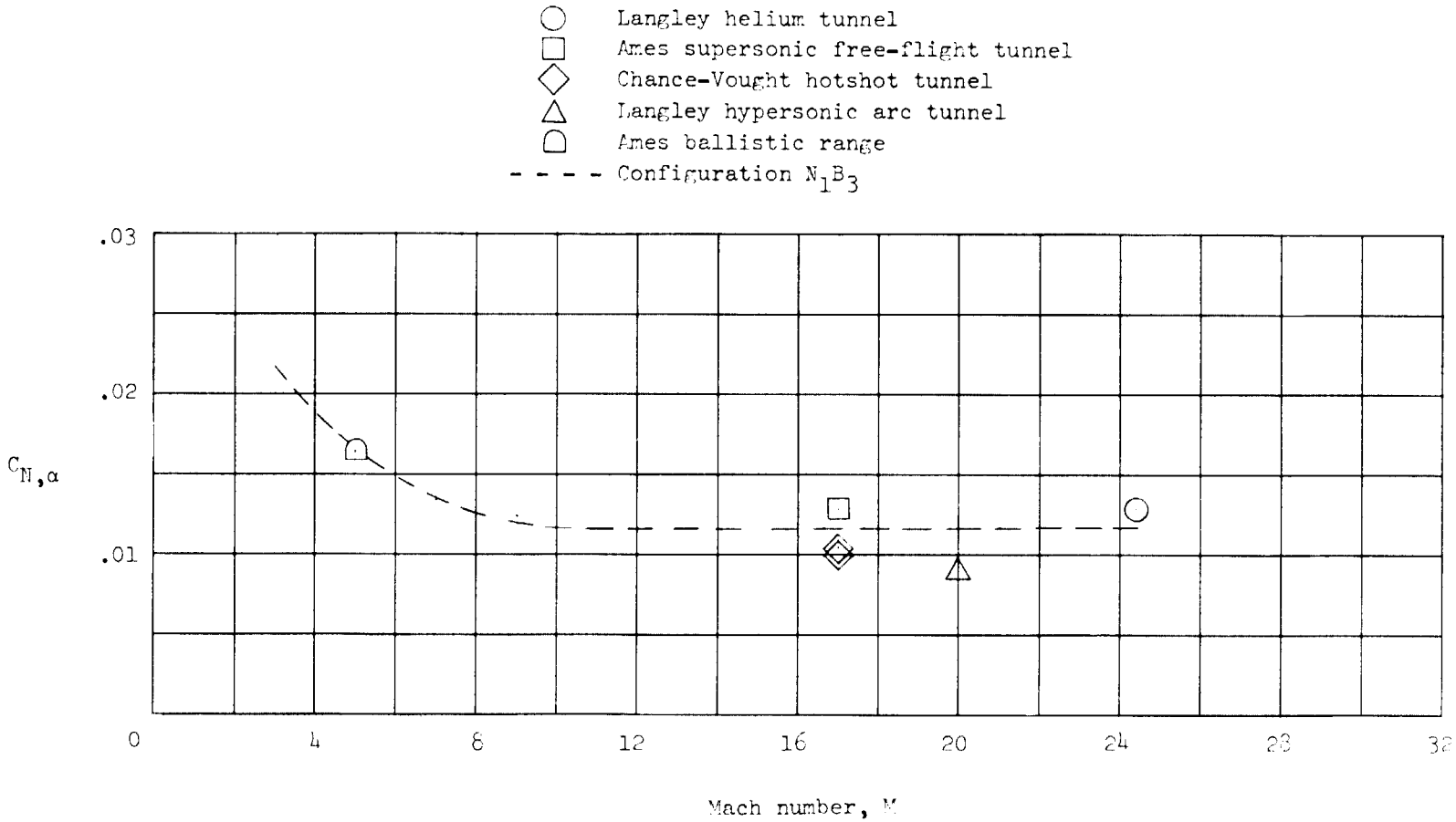

(a) Effect of Mach number on $C_{N,\alpha}$ of configuration N_4B_4.

Figure 16.- A summary of the longitudinal stability results of configuration N_4B_4 at hypersonic speeds.

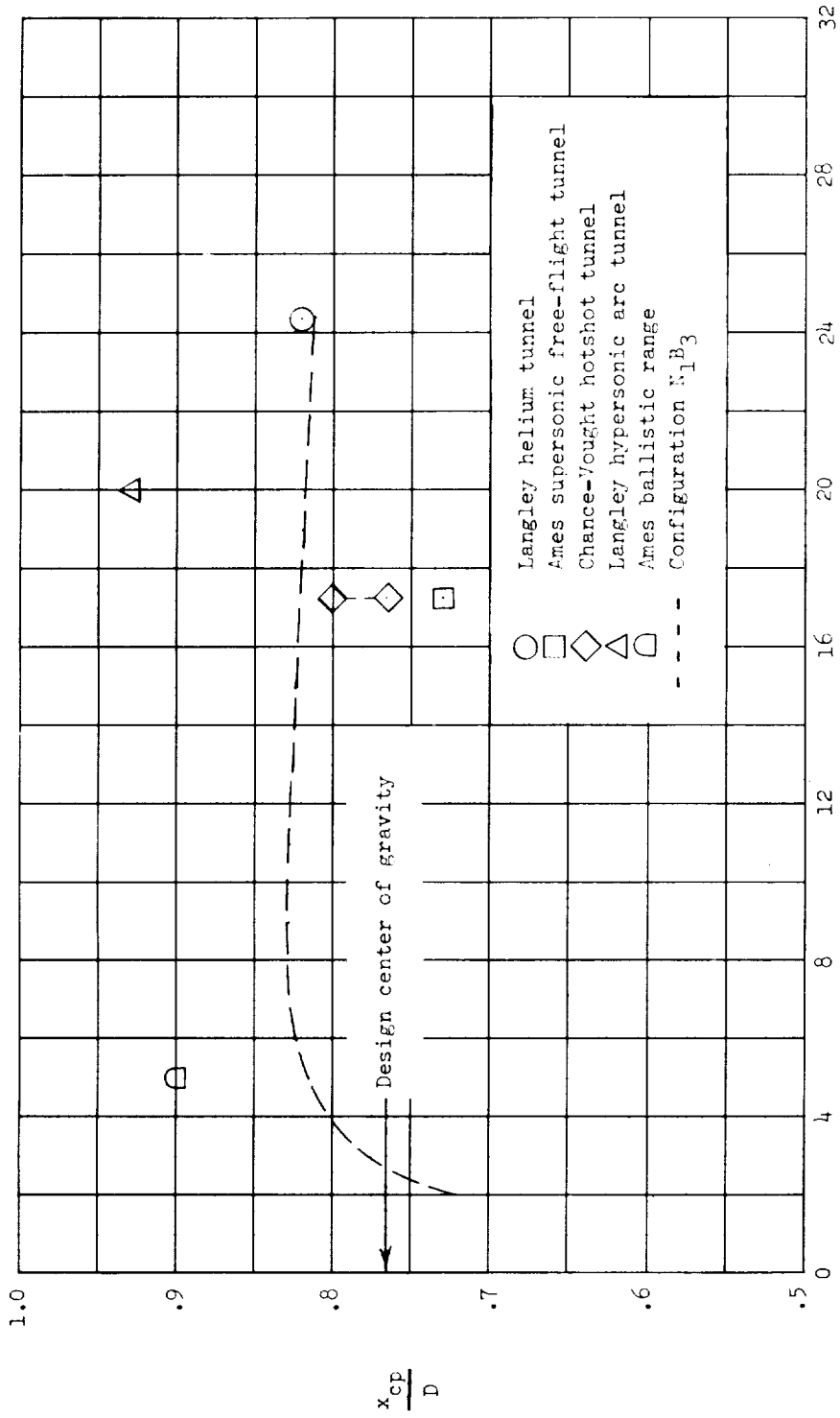

(b) Effect of Mach number on $\frac{x_{cp}}{D}$ of configuration N_4B_4.

Figure 16.- Continued.

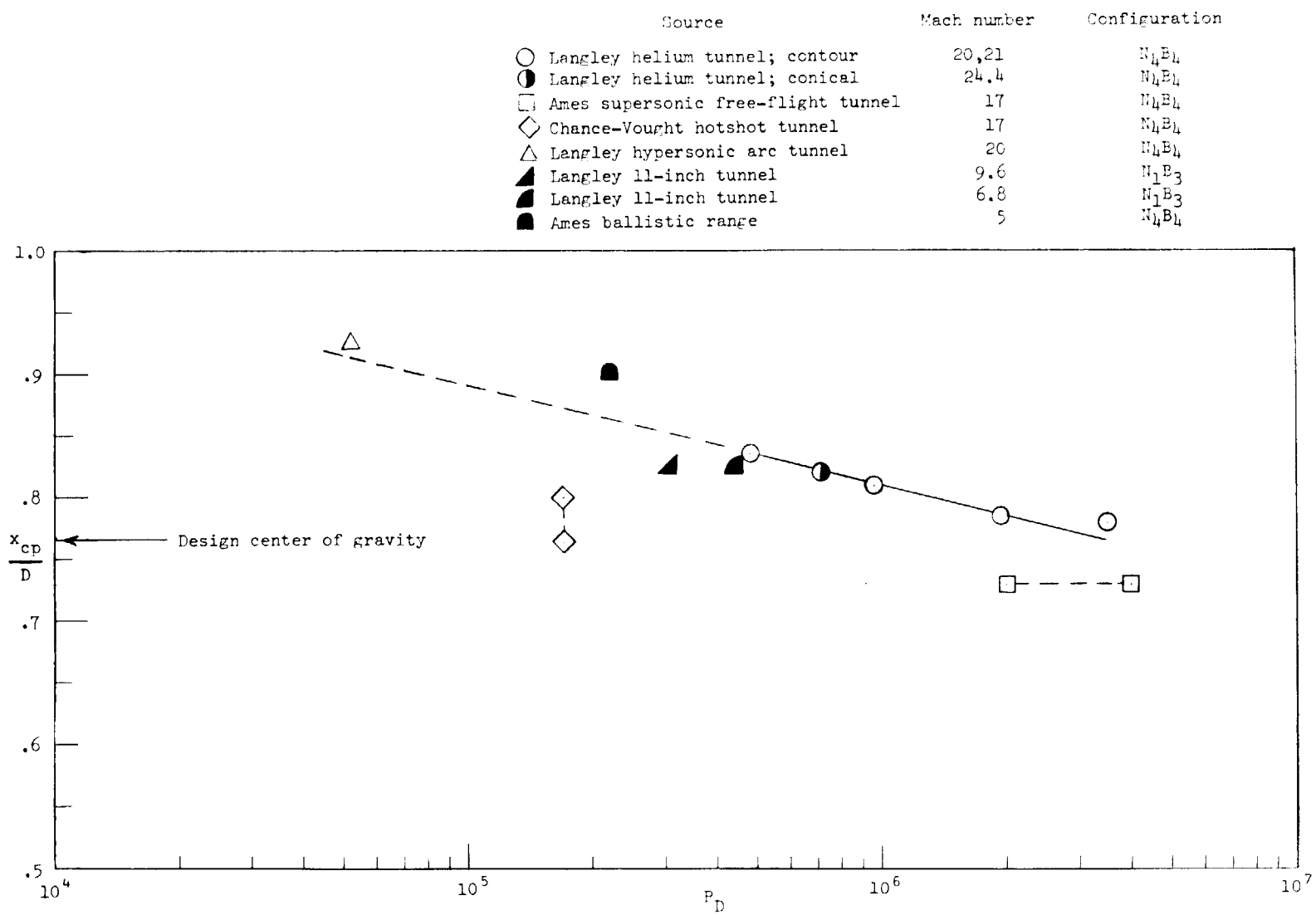

(c) Effect of Reynolds number on $\frac{x_{cp}}{D}$ of configuration N_4B_4. Solid symbols represent "low" hypersonic Mach number data.

Figure 16.- Continued.

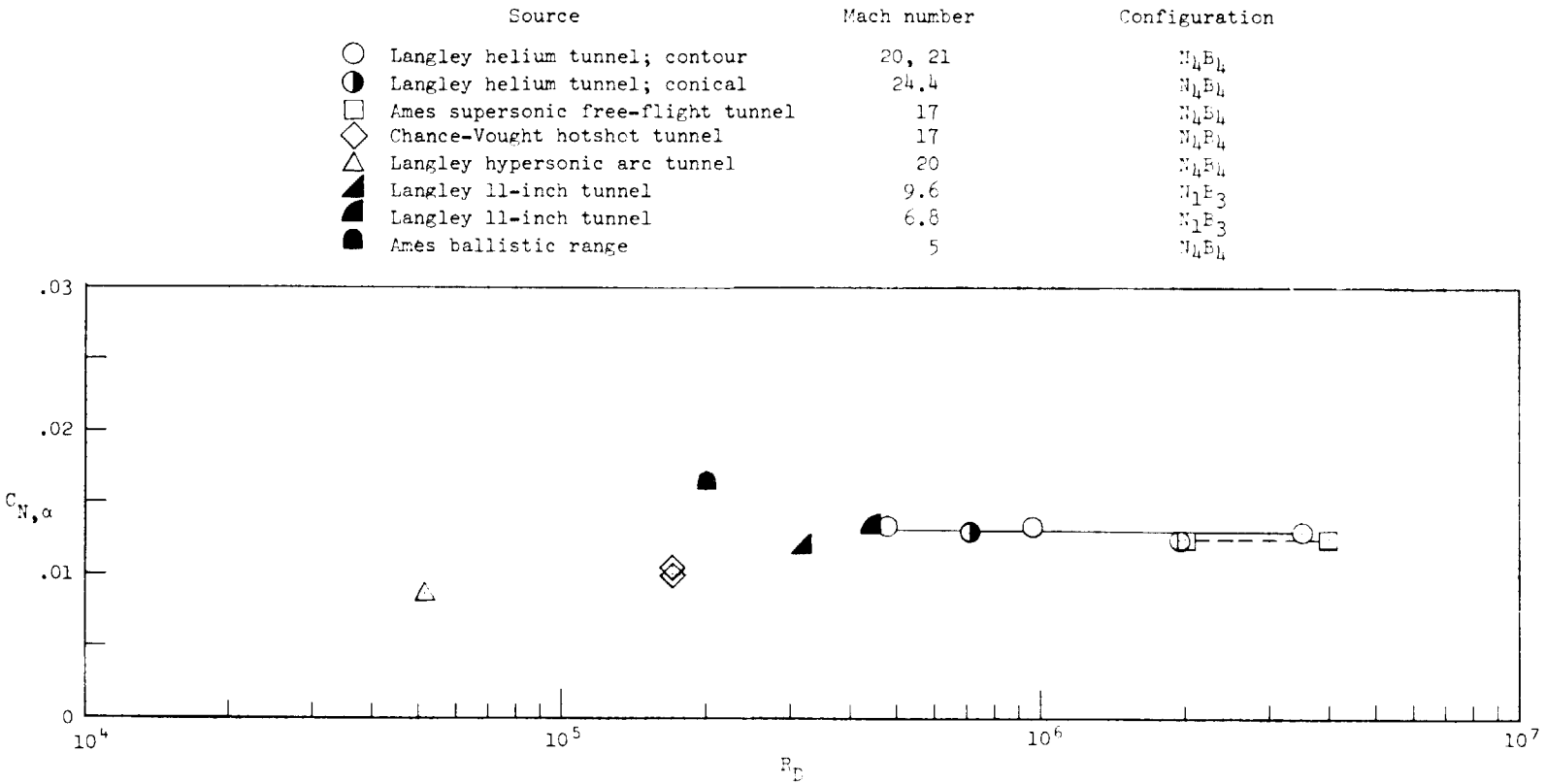

(d) Effect of Reynolds number on $C_{N,\alpha}$ of configuration N_4B_4. Solid symbols represent "low" hypersonic Mach number data.

Figure 16.- Concluded.